Sl. No.	INDIAN INSTITUTE OF TECHNOLOGY ROPAR List of Recent Publications with Abstract Coverage: November, 2024
A	**Book Chapter(s)**
1.	A comprehensive analysis of cell balancing in BMS for electric vehicle **R Sarker, S Datta, K R Singh**, A K Das - Sustainable Mobility: Policies, Challenges and Advancements: Book Chapter, 2024 **Abstract:** In recent years, the technology behind electric vehicles has advanced to become revolutionary. Since it is proved to be the brain of the battery pack, the most crucial element of an electric vehicle (EV) in the automobile industry is the battery management system (BMS). The main duty of the BMS is to carefully monitor the battery's health, which ensures the dependable operation and increases battery performance. This paper explains the BMS and how the different cell balancing works and how to equalize the state of charge (SOC) of a multi-battery cell. Active and passive cell balance are the two different types of cell-balancing strategies. Instead of discharging with the extra potentials to a bleeding resistor as is the case with a passive cell equalizer, an active cell equalizer implies moving the potential from a higher-potential cell to a lower-potential cell. Additionally, a passive cell equalizer or balancer wastes the charge, reducing the effectiveness of a cell balancer with the topology. So, balancing of the batteries also depends upon accurate SOC estimation. However, the energy transferring while balancing active cells results in higher efficiency compared to passive balancing.
2.	Artificial intelligence and machine learning in industry 6.0 S Pattanaik, M Mohammed, **V Sood** - Industry 6.0: Technology, Practices, Challenges, and Applications: Book Chapter, 2024 **Abstract:** The synergy of artificial intelligence (AI) and machine learning (ML) drives Industry 6.0, marking a paradigm shift in industrial technologies. This phase brings in a new era of intelligent automation, based on data insight, as well as adaptive industrial processes, which will revolutionize the way in which industries work and evolve. Our objective in this abstract is to analyze the transformative effect that machine learning and AI will have on Industry 6.0. Specifically, we will look at important applications like predictive maintenance, personalized production, and streamlined supply chains. In addition, we explore the problems and considerations that are inherent in the deployment of these technologies. These include ethical difficulties, the necessity for worker reskilling, and the demand for responsible administration of artificial intelligence development. It is feasible for companies to attain previously inconceivable levels of efficiency, agility, and innovation by using the power of artificial intelligence and machine learning. This will usher in a future in which human-machine collaboration will fuel sustainable progress and prosperity. Artificial intelligence (AI) and machine learning (ML) technologies have been incorporated into a variety of different enterprises, which has resulted in a transformation of those industries and opened the way for enhanced efficiency, innovation, and competitiveness. We study the significant influence that artificial intelligence and machine learning have had across several sectors, concentrating on the most noteworthy applications and successes. From predictive analytics in healthcare to predictive maintenance in manufacturing, AI and ML algorithms are generating important advances, enabling firms to make data-driven choices, optimize operations, and reveal new opportunities. However, the widespread use of these technologies also resulted in the rise of a variety of obstacles, such as ethical considerations, concerns about privacy, and the demand for skilled individuals. It is conceivable for sectors to attain new levels of development, resilience, and sustainability in the digital era

	provided they are able to overcome these hurdles and fully utilize the promise of artificial intelligence and machine learning. The objective of this abstract is to offer a detailed study of the role that artificial intelligence and machine learning play in defining the future of industry. It underlines the importance of regulated deployment and responsible governance in order to fully achieve the revolutionary potential of these technologies.
3.	Biomedical applications of biogenic carbon-based fluorescent nanoparticles **K Kaur, G Singh**, R Badru, N Kaur, **N Singh** - Biogenic Nanomaterial for Health and Environment: Book Chapter, 2024 **Abstract:** The wide-ranging applications of carbon dots (CDs), which can be developed using either green or chemical precursors, have been made possible due to their reported properties and the various precursors that have been identified. This has opened up new opportunities for the development of high-quality CDs and their use in optoelectronic devices, bioimaging, and other applications. Green precursors can be derived from fruits, vegetables, flowers, leaves, seeds, stems, crop residues, fungi/bacteria species, and waste products, while chemical precursors can be categorized as either acid reagents or non-acid reagents. It provides a brief review of the past ten years of CD synthesis using both green and chemical precursors, as well as the use of CDs as sensing materials in biomedical applications. This comprehensive review will be a valuable resource for researchers who are interested in synthesizing high-quality CDs for a variety of applications.
4.	Carbon quantum dots, a novel theranostics nanoprobe in biomedical engineering **A Ghosh**, U Basu, M Bhatt, T K Ghosh, **B Das** - Nanomedicine in Translational Research: Book Chapter, 2025 **Abstract:** Carbon quantum dots (CDs) are an emerging class of nanomaterials that have been reported to have unbound potential for drug delivery and biosensing. Fluorescent nano-sized CDs have been utilized in bioimaging for their excellent optical properties, high biocompatibility, and low toxic effects combined with chemical inertness and cytotoxicity. CDs are usually less than 10 nm in size and are luminescent with some form of surface passivation. The optical properties of carbon-based nanodots have gathered much attention in the research community for their wide variety of potential applications in optoelectronics. CDs have been pursued more extensively for the lack of a classical quantum confinement effect, which makes them highly active but ensures nontoxic consequences. Some of the various aspects of CDs and their recent developments and research in the biomedical and biotechnology field have been discussed. The review also focuses on how computational biology can transmute and enhance research on nanoparticles, especially CDS, and give an extensive idea about particle binding, affinity, characteristics, and optical and electrical properties that can be suitable for further wet-lab research purpose.
5.	In vitro systems to demonstrate the nano effect (scope: In vitro systems to demonstrate the efficacy and safety of biomaterials for nanomedicine applications) **S Yadav, S Naidu, B Das** - Nanomedicine in Translational Research: Book Chapter, 2025 **Abstract:** Nanomedicine constitutes a medicinal discipline wherein nanomaterials (1–100 nm) are utilized for diagnostic, imaging, and therapeutic interventions. A diverse array of novel nanomaterials, encompassing lipidic, carbon-based, polymeric, and inorganic nanoparticles have been developed for various biomedical applications. Studies reported physico-chemical properties of these nanomaterials may exhibit toxicity upon human exposure. Thus, it is crucial to evaluate the safety and efficacy of nanomaterials for medicinal applications. Various In-silico approaches have been developed for toxicity screening of nanomaterials. Currently, there is a growing emphasis on in-vitro studies for nanomaterial toxicity assessment due to low cost and reduced animal experimentation. In this chapter, we have summarized, conventional and

	advanced approaches for the safety evaluation of nanomaterials intended for use in nanomedicine.
B	**Conference Proceeding(s)**
6.	A fast multilevel vulnerability assessment strategy for power systems cyber security **S Agarwal, R Sodhi** - 2024 IEEE 4th International Conference on Sustainable Energy and Future Electric Transportation (SEFET), 2024 **Abstract:** This paper proposes a simple and fast method to assess the vulnerable attack path in a power system, which an attacker can take to create maximum damage in the system. The maximum damage is assessed based on the load disruption caused, or the island formed as a consequence of the attack. Since an attacker may need to launch the attack multiple times (termed as multilevel) to achieve the desired disruption, finding the critical path becomes a multilevel exploration task. During each level- i , the attacker's target becomes to identify the most vulnerable lines/outages of the system. In this work, a three-step scheme is developed wherein, Stage-1 identifies the location of vulnerability using graph theoretical concepts of nodal betweenness centrality (NBC) and node load capacity (NLC). Stage-2 estimates the cascading failures based on the impact caused by the N−k−{i} outages in the system and Stage-3 finally identifies the critical path. The proposed methodology is tested on the IEEE 14-bus system. Based on the results obtained, it is inferred that by incorporating the concepts of NBC and NLC, the process of finding critical path becomes much easier and faster than the traditional methods that utilise load flow studies for finding the same.
7.	A multilevel vulnerability assessment strategy of N-k-{j} contingencies for ensuring the cybersecurity of power systems **S Agarwal, R Sodhi** - 2024 IEEE 4th International Conference on Sustainable Energy and Future Electric Transportation (SEFET), 2024 **Abstract:** This paper proposes a reliable method for identifying vulnerable attack paths in a power system from the perspective of the system operator. The goal is to infer the potential disruption that can be caused by an attacker with single or multiple consecutive attacks under different loading scenarios. The assessment of damage is contingent upon the load disruption incurred and the system's attainment of a non-convergent state or the formation of an isolated island as a repercussion of the attack. The proposed method is a multilevel exploration task that identifies the most vulnerable lines in the system during each level. The method uses a two-step scheme, wherein Stage-1 identifies vulnerable lines using a novel multilevel vulnerability assessment index based on modal analysis and participation factors during N−k−{j} outages, and Stage-2 recognizes the explored vulnerable attack path(s). The method is tested on the IEEE 14-bus system and proves to be effective in terms of both time efficiency and simplicity.
8.	Application of genetic programming in the field of geotechnical engineering- A review **NJ Sahare, M Raheena** - Indian Geotechnical Conference, 2024 **Abstract:** Geotechnical Engineering largely focuses on the complex nature of soils and rocks. Because this complexity creates a high level of ambiguity in the imitation of these materials' nature. Genetic Programming (GP) has been initially developed by Koza (Genetic programming: on the programming of computers by natural selection. MIT Press, Cambridge (MA), 1992) and then used by many researchers in different areas including geotechnical engineering. This paper closely reviewed the application of GP in some areas of geotechnical engineering identified: settlement of the shallow foundation, bearing capacity of pile foundation, liquefaction assessment, estimation of pore water pressure, compaction parameters (OMC & MDD), soil-fiber composite assessment, free swell and swell pressure, the effectiveness of rolling dynamic compaction, prediction of soil water characteristic curve, and unconfined compressive strength

	(UCS). GP has been getting success over the years, because of its ability to find the relationship between the input variable and predict the output variable. This paper also discusses the future scope of GP in some unexplored areas of geotechnical engineering.
9.	Applications of solar energy: energy storage, cooling, and water desalination **J Dwivedi, KS Chauhan, R Beniwal, AS Kashyap, H Tyagi** - Turbulence & Energy Laboratory Annual Conference, 2024 **Abstract:** This paper presents the results of various applications of solar energy in the field of thermo-fluids engineering, specifically in the following 3 topics: energy storage, cooling, and water desalination. In the first part, the result of using PCM (phase change materials) for storage solar energy as sensible and latent energy in conjunction with nanoparticle-laden fluids is presented. It is seen that for medium-temperature range energy storage, the materials and geometry can be adjusted in order to tune the charging and discharging processes at much higher efficiencies. The second part of the paper presents results of low-cost cooling techniques which avoid the use of high-energy consuming VCR (vapor compression refrigeration) cycles, and instead use solar energy as the driving force, leading to more environmental friendly cooling solutions. In the third and final part of this paper, the solar energy-driven desalination process of membrane distillation has been presented in detail. Here, the main parameters of concern are the distillation flow rate as well as the overall GOR value (Gained Output Ratio). It is observed that solar-driven desalination processes can avoid the use of high grade energy (such as electricity) and can instead be operated using low grade energy source such as solar energy.
10.	Can threshold memory switching memristor be effectively utilized for the hardware implementation of brain-inspired Neuromorphic systems? **MS Yadav, B Rawat** - 2024 International Semiconductor Conference (CAS), 2024 **Abstract:** Integration of the threshold-type selector layer with the memristor device (TS-MS) has emerged as a promising candidate for suppressing the undesired sneak path current within crossbar memory structures. However, their potential advantages for neuromorphic computing architecture remain unexplored. In this context, we systematically explore the device-to-crossbar level performance of NbO 2 -HfO x -based TS-MS cell with multi-state resistive switching behavior in a layer neural network for pattern recognition. The NbO 2 -HfO x -based TS-MS device demonstrates the existence of distinct four-level resistance states during the reset process, which facilitates electronic synapses with a high resistance state modulation within the range of 6.5 KΩ to 25.71 KΩ and an on-off resistance ratio of 12. The crossbar simulation reveals that TS-MS could allow recognition accuracy with around 62% when the noise level increases around 27%. Our findings highlight that TS-MS devices have the potential to offer noise immunity operations, coupled with energy efficiency, which positions them as strong candidates for future hardware implementations of brain-inspired neuromorphic systems.
11.	Characterizations of cyclic combustion variations in RCCI engine using multifractal detrended fluctuations analysis **RK Yadav, MR Saxena, RK Maurya** - International Conference on Advances in Energy Research, 2024 **Abstract:** This study experimentally investigated the cyclic variations and partial burn in reactivity-controlled compression ignition (RCCI) engines. Multifractal Detrended Fluctuations Analysis (MFDFA) is employed for the purpose of describing cyclic variations and partial burn. The experiments are carried out on a modified diesel engine. Diesel is injected directly into the cylinder, whereas petrol is introduced into the inlet manifold via the port-injection system to facilitate RCCI combustion. This study explores the influence of the gasoline/diesel premixing ratio r_p on combustion stability and partial burn. It was found that the cyclic variations in CA_{10},

	CA_{50}, and COV_{IMEP} increased with r_p. Results indicate that the percentage of misfiring cycles increased from 36.4% to 83.1% when r_p increased from 40 to 50%. MFDFA analysis shows that total heat release (THR) time series becomes anti-persistent and its degree of multifractality decreases with r_p. The multifractal analysis also shows that THR, $CA_{10,}$ and CA_{50} have large fluctuations at smaller scales, and these fluctuations are persistent in nature, while smaller fluctuations at large scales are anti-persistent in nature.
12.	Cluster-wise response aggregation-based differentially private pool energy market model S Dash, **R Sodhi**, SN Singh - 2024 IEEE 4th International Conference on Sustainable Energy and Future Electric Transportation (SEFET), 2024 **Abstract:** This paper [1 1] A full financial support is provided in the Core Research Grant by the Science and Engineering Research Board (SERB), India, under IIT Ropar project no. CRG/2018/000084, to carry out this research work. proposes a differential privacy (DP) mechanism for the decentralised pool-based local energy market (PEM) model in the distribution grid. Many traditional PEM models employ alternating direction method of multipliers (ADMM) to reduce the confidential information sharing between participants and energy market operator (EMO). However, an EMO/Aggregator with malicious intent or any cyber-attacker reading the communication between the EMO and participants can still infer the value by looking into their responses over a large time-span. To address the challenge, the proposed DP mechanism completely masks these shared exact information without altering the PEM output from the traditional one. The masking is achieved by three stages, namely 1) clustering, 2) random sharing, and 3) aggregation. The efficacy of the proposal is validated using the Pecan street dataset on MATLAB with Gurobi solver, and a very high degree of DP is observed without any loss of optimality in PEM clearing.
13.	Effect of different gas nanobubbles on fermentation pattern of yoghurt starter culture S Sirame, P Singh…**N Nirmalkar** - The 5th International Electronic Conference on Foods session Innovation in Food Technology and Engineering, 2024 **Abstract:** Nanobubbles (NBs) have attracted great attention recently, offering a wide range of applications across various disciplines due to their unique properties. Fermentation is an age-old practice carried out for the preservation of milk and milk products, stirred yoghurt being one such product. In the present study, it was attempted to understand the effect of the incorporation of nanobubbles on the fermentation pattern of yoghurt starter culture (YSC) i.e., *Streptococcus thermophilus* and *Lactobacillus bulgaricus*, and the quality attributes of yoghurt thus prepared. Different types of NBs were prepared using compressed purified air, CO_2, O_2, and N_2 in water and milk systems using a bulk nanobubble generator. Average bubble concentration was found to be $\sim 10^7$ mL^{-1} while mean size was found to be 176.0 ± 3.5nm to 217.6 ± 6.9nm. It was observed that the types of NBs had a significant effect on the metabolism and microbial growth of the starter culture. Among the four different types of NBs, CO_2-NBs had a significantly positive effect on bacterial cell mass growth besides increasing viability in fermented milk. Our findings suggest that NB in general and CO_2-NB in particular have the potential to alter the fermentation pattern in fermented dairy products. Further, concerning the quality attributes of NB-incorporated stirred yoghurt, notable changes were observed in terms of viscosity, mouthfeel, and shelf life. A significant increase in viscosity of the NB-incorporated stirred yoghurt was observed as compared to the control sample, which may be attributed to milk protein–polysaccharide interaction at the interface of NBs. It is therefore concluded that NB technology has the potential to be applied as a new processing tool to easily tweak the fermentation pattern and physicochemical properties of fermented dairy products to meet the increasing consumer demand for innovative products with variable consistency and functionality.

14.	Evaluation of optimum wall slope of a frustum shape solar pond under variable ambient conditions S Verma, **A Singh, R Das -** 3rd IEEE International Conference on Power Electronics, Intelligent Control and Energy Systems, ICPEICES, 2024 **Abstract:** A transient model is presented in connection with a frustum-shape solar pond for a one-year period. The pond area at top is taken to be sufficiently large such that wall shading effect is ignorable. Implicit finite difference method (FDM) has been used to solve the governing energy equation. Using this solution, temporal variation of lower-convective zone (LCZ) temperature is observed for different wall slopes, keeping the total pond volume and topmost area constant. It is seen that under mentioned constraints, LCZ temperature at every instant is larger for a larger wall slope. Thus, the best possible solar pond is attained at theoretically infinite wall slope, dignifying a cylindrical pond. Hence, the conclusion observed by the authors in previously published steady state model of the literature is reported to be true even for transient state, which is that a vertical walled solar pond is the best shape for maximum thermal output.
15.	Explaining the identification of granular crack with deep learning and XAI **A Pratap, N Sardana** - 2024 IEEE Region 10 Symposium (TENSYMP), 2024 **Abstract**: Precise detection of granular fractures is crucial for various engineering applications, and Deep Learning approaches can transform imaging methodologies and material analysis. This study employed a convolutional neural network (CNN) that incorporated explainability elements to improve the trustworthiness and transparency of the model in classifying granular cracks. After conducting thorough model comparisons and analyses, a bespoke model was chosen. Extensive model comparisons and analyses led to the selection of a custom model with 91% training accuracy and optimized parameters. Fine-tuning of six pre-trained models identified VGG-16 as the top performer, achieving 99.96% training accuracy and 97.7% testing accuracy. Explainable AI (XAI) techniques, particularly the insertion method, provided robust interpretability, with attributed scores of 0.96 for insertion, 0.69 for deletion, and 0.37 for fidelity. Visualization using various attribution mapping methods reinforced the trustworthiness of this work in granular crack identification.
16.	Exploring the potential of a 1T-1M HfO_X-based resistive switching device for articulating artificial neural network hardware **S Gupta, MS Yadav, VK Tavva, B Rawat** - 2024 International Semiconductor Conference , CAS, 2024 **Abstract:** In this work, we investigate the pattern recognition accuracy and energy consumption of crossbar architectures based on HfO X -based one-transistor one-memristor (1T-1M) cells, utilizing a fully calibrated analytical model. Our results highlight the uniform and well separated low resistance states (LRS) with HfO X -based 1T-1M cells provide excellent noise-immune operations with a recognition accuracy of approximately 47% in the presence of a 26% noise level. Further, the HfO X -based crossbar array maintains an average energy consumption of around 18 nJ during data storage within each cell. Finally, the artificial neural network designed with 1T-1M demonstrates the 90% recognition capabilities in handwritten MNIST digits.
17.	Impact of misalignment on wearable arm robotic system **Bhavna, E Singla, DK Mahajan** - International and National Conference on Machines and Mechanism, 2024 **Abstract:** With the advancement of wearable robotic systems, several issues have been observed, and one significant concern is the misalignment between human joints and exoskeleton joints. The present study focuses on analyzing the impact of kinematic mismatch and misalignment in

	wearable robotic systems by considering contact and constraint reaction forces at joints, as well as the required moments to execute primary movements of the human arm. The primary focus is on the key activity of flexion/extension motion of the human arm and examines two configurations of an exoskeleton coupled with the human arm. In configuration 1, a 2-degree-of-freedom exoskeleton is used, with one degree of freedom at the shoulder joint and one at the elbow joint. These degrees of freedom are aligned to correspond with the shoulder and elbow joints of the human arm in the coupled model. In configuration 2, modifications have been made to the exoskeleton to account for the complexity of the human shoulder, which has five degrees of freedom. In this modified version, five revolute joints at the shoulder joint are included to mimic the shoulder's five degrees of freedom. This modified exoskeleton is expected to be more compatible and accurately replicate the motion of the human arm.
18.	Inverse prediction of unknown parameters for a geothermal/waste heat operated Kalina Cycle **A Singh**, **R Das** - 3rd IEEE International Conference on Power Electronics, Intelligent Control and Energy Systems, ICPEICES, 2024 **Abstract:** In this work, an inverse problem pertaining to the estimation of the operational parameters (OPs) in a low-temperature heat source-driven Kalina cycle (KC) is solved. First, a forward model is used to simulate the KC's steady-state response at various temperatures associated with the superheater (T^{Sup}) and absorber (T^{Abs}), as well as at different strong solution concentrations (X^{Ss}). It is observed that the forward analysis yields the same set of OPs for any optimization target when the net exergy flow rate into the KC system remains constant. This implies that the choice of objective function has no bearing on the optimization process as long as the conditional statement of fixed exergy input is satisfied. A dragonfly algorithm-based inverse analysis is then carried out on the KC system. The research is expected to be useful in choosing KC system's OPs from a range of viable options that can satisfy a desired objective.
19.	Pebble guided rendezvous despite fault **A Saxena**, B Gorain, S Mandal, **K Mondal** - International Symposium on Stabilization, Safety, and Security of Distributed Systems (SSS), 2024 **Abstract:** We consider the rendezvous problem in an anonymous port-labelled connected simple graph. The objective is for two mobile agents to meet at some node of the graph without prior knowledge of the graph or the other agent's position. An oracle, that knows the graph and the starting positions of the agents, helps the agents by placing identical pebbles, at most one per node at some of the nodes. We introduce faults by considering the presence of a single faulty node that may remove a pebble that is kept on the node, or may add a pebble where there was no pebble placed by the oracle. The position of the faulty node is unknown to the agents as well as the oracle. Our goal is to find an efficient rendezvous algorithm regardless of the number of pebbles placed by the oracle in the presence of a faulty node. For trees, we present an algorithm that uses $O(D\log\Delta)$ pebbles and runs in time $O(D\log\Delta)$, where Δ is the maximum node degree and D is the shortest path distance between the initial agent positions. We prove that our algorithm for trees is optimal in terms of time. Additionally, we study the problem in general graphs with the constraint that the initial agent positions are no more than distance three apart. We propose an algorithm using $O(\log\Delta)$ pebbles with run time $O(\log^3\Delta)$.
20.	Temperature and fluid velocity field estimation in melt-pool using multiphysics-based numerical simulation for multi-track selective laser melting process **R Kumar,** A Rajput, **A Agrawal** - International Conference on Processing and Fabrication of Advanced Materials, 2024 **Abstract:** The selective laser melting (SLM) process involves various physics-based phenomena with many process variables, so predictions of its characteristics and part quality are tedious. Researchers are developing numerous numerical and analytical formulation models to simulate

	the SLM process realistically and efficiently to compute various functions and part characteristics. The present work developed a fully developed Multiphysics 3D Finite Element numerical model for the multi-track SLM process by incorporating transient heat transfer, fluid flow, Marangoni effect, and material phase transformation. The porosity and deformation behavior of the powder bed is also considered to replicate the possible contraction in the powder bed. The temperature-dependent material properties of Ti6Al4V alloy were used to run the simulation. The temperature and velocity distribution obtained after incorporating fluid behavior and Marangoni convection gives the final melt-pool dimensions by extrapolating the temperature isotherms. Melt-pool dimensions increase with the subsequent tracks due to higher temperature regions in consecutive tracks, which further stabilizes once it attains steady-state temperature. The model can be further improved to study the part distortion and residual stresses in the SLM process.
21.	Triply periodic minimal surface (TPMS) metamaterial exhibiting simultaneously superior acoustic and mechanical energy absorption performance **R Dewangan, N Kumar** - ISME International Conference on Advances in Mechanical Engineering, 2024 **Abstract:** The advancement of 3D printing has created new opportunities for producing innovative materials with distinctive features, such as microlattice metamaterials. These materials might be more effective than conventional materials. Particularly, there is a demand for materials that are lightweight, resilient, and effectively sound transmission loss, making them beneficial for real-world engineering applications. However, there has not been much study on metamaterials that can perform both of these functions at once. In this study, we propose TPMS (Triply Periodic Minimal Surface) metamaterials that perform exceptionally well at absorbing mechanical and acoustic energy. In which a novel idea for the particular structural design and material choice of metamaterials with dual sound transmission loss and mechanical energy absorption capabilities is put forth. In order to understand more about the TPMS structure's performance and variations in mechanical energy absorption as a function of strain rate, it is also investigated how it behaves under various strain rates.
22.	Visible to Near-IR Tunable Plasmons in Nanoporous gold films **J Singh, S Sarkar** - 2024 18th International Congress on Artificial Materials for Novel Wave Phenomena, Metamaterials, 2024 **Abstract:** This study explores the synthesis and characterization of nanoporous gold (NPG) films fabricated using a straightforward chemical etching method. Atomic force microscopy (AFM) was employed to examine the surface morphologies of NPG samples with varying film thicknesses, revealing a progressive transition from plain gold films to nanoporous structures as the thickness increases. Analysis of root-mean-square roughness (RMS) and porosity unveiled a significant dependence on film thickness, underscoring the intricate interplay between etching kinetics and film growth dynamics. Additionally, UV-Vis characterization in reflection mode showcased the tunability of plasma edge and plasmon frequency, suggesting the potential for customizing optical properties through film thickness adjustment. Overall, this research provides valuable insights into the controlled synthesis and characterization of NPG films, with implications for applications in plasmonics, sensing, and beyond.
C	**Journal Article(s)**
23.	A double serpentine channel liquid cooling plate for hotspot targeted cooling of lithium-ion batteries in a battery module **D Yogeshwar**, R Repaka, **NK Marath** - International Journal of Thermal Sciences, 2025 **Abstract:** The study presents the development and performance analysis of a novel double serpentine channel cooling plate aimed at enhancing heat dissipation from hotspot-targeted

	cylindrical lithium-ion batteries within a battery module. Specifically, the research focuses on the comparative evaluation of the cooling performance between the double serpentine and single serpentine channel designs. Key parameters such as battery discharge rate, coolant flow velocity, and aluminum nanoparticle concentration are analyzed to evaluate their impact on battery thermal management. Finite element simulations are conducted to model thermal energy generation, fluid flow dynamics, and heat transfer behavior within the battery module. The results demonstrate that the single serpentine channel cooling plate (SSC-CP) reduces the maximum battery module temperature by 4.04 K and 11.01 K at 1C and 2C discharge rates, respectively, compared to natural cooling. Further enhancement in heat dissipation is observed with the incorporation of nanoparticles in the cooling fluid and an increase in coolant flow velocity. Additionally, the double serpentine channel cooling plate (DSC-CP) offers further improvement in thermal management by targeting hotspots within the battery module. Specifically, the DSC-CP reduces the maximum battery module temperature compared to the SSC-CP from 304.78 K to 303.70 K at 1C and from 304.89 K to 303.09 K at 2C. Furthermore, the DSC-CP reduce ΔT, the difference between the maximum and minimum temperature of the battery module, from 5.73 K to 4.69 K at 1C and from 6.97 K to 4.65 K at 2C, thereby improving temperature uniformity and reducing thermal gradients.
24.	A low-power common-mode insensitive rail-to-rail dynamic comparator for ADCs **N Sharma**, RK Srivastava, D Sehgal, **DM Das** - Integration, 2025 **Abstract:** This paper presents a low-power, high-speed dynamic comparator with a rail-to-rail input common-mode ($V_{i,cm}$) range. The proposed comparator has high-speed performance throughout the 0-Vdd $V_{i,cm}$ range, thus attributing common-mode insensitivity. This work introduces a merger of NMOS and PMOS dynamic pre-amplifiers with a modified latch to achieve the rail-to-rail $V_{i,cm}$ operation. A novel activation clock logic is also proposed, activating only one pre-amplifier based on the $V_{i,cm}$ value and ensuring low-power consumption and provides reduction of 17% in the energy per conversion as compared to the comparator without activation clock logic. The proposed comparator is designed using 65-nm CMOS technology with a 1.2 V supply voltage and is operating at 1 GHz frequency. We have presented the analytical models of the delay and offset which is verified with the rigorous post-layout simulation results. To validate the robustness of the proposed comparator, the PVT corner analysis with Monte Carlo simulation is also performed for different $V_{i,cm}$.
25.	A multi-level adaptive mesh refinement strategy for unified phase field fracture modeling using unstructured conformal simplices **A Pandey, S Kumar** - Computer Methods in Applied Mechanics and Engineering, 2025 **Abstract:** The phase field model (PFM) has emerged as a popular computational framework for analyzing and simulating complex fracture problems. Despite PFM's inherent capacity to model relatively complex fracture phenomena such as nucleation, branching, deflection, etc., the computational costs involved in the analysis are quite high. Hence, a multi-level adaptive mesh refinement framework is proposed for a unified phase field model (PFCZM) to improve the computational efficiency. The proposed adaptive framework can be implemented for structured as well as unstructured meshes, making it suitable for analyzing complex fracture problems. This framework adaptively generates local mesh refinement at the discrete crack tip, based on an active element error indicator, until the damage is initiated, hence completely avoiding the pre-requisite of local mesh refinement. Further, the gradient of energy degradation and the gradient of dissipated fracture energy based error indicators are proposed to capture the fracture domain and regions ahead of the crack tip, respectively. The Newest vertex and Maubach's refinement routines are implemented as the element level-based hierarchical refinement strategies. Unlike recently proposed adaptive strategies for PFCZM involving elements with hanging nodes, the proposed adaptive framework inherently addresses the conformity and reflectivity of the discretized domain efficiently. The robustness and accuracy of the framework

	is checked against four benchmark fracture problems, demonstrating a significant reduction in computational costs with sufficient accuracy.
26.	A novel polyurethane-based silver foam dressing with superior antimicrobial action for management of infected chronic wounds **JH Rajput**, **V Rathi**, **A Mukherjee**, P Yadav, T Gupta, **B Das, A Poundarik** - Biomedical Materials, 2024 **Abstract:** Wound healing is a complex and dynamic process supported by several cellular events. Around 13 million individuals globally suffer from chronic wounds yearly, for which dressings with excellent antimicrobial activity and cell viability (>70%, as per ISO 10993) are needed. Excessive use of silver can cause cytotoxicity and has been linked to increasing antimicrobial resistance. In this study, HDI Ag foam was synthesized using a safer hexamethylene diisocyanate-based prepolymer (HDI prepolymer) instead of commonly used diisocyanates like TDI and MDI and substantially lower Ag content than that incorporated in other Ag foams. In vitro characteristics of the HDI Ag foam were evaluated in comparison with leading clinically used foam-based dressings. All dressings underwent a detailed characterization in accordance with industrially accepted BS EN 13726 standards. The HDI Ag foam exhibited highest antimicrobial efficiency against *S. aureus* and *P. aeruginosa* (static condition), with the lowest amount of Ag (0.2 wt%) on the wound contact surface. The extracts from HDI Ag foam showed superior cell viability (>70%), when tested on the L929 mouse fibroblast cell line. Measurements of moisture vapor transmission, fluid handling, physico-chemical and mechanical properties ensured that the HDI foam was clinically acceptable for chronic wound patients.
27.	An improved Ac supply based method for measuring the inductance profile of SRM using SOGI **Z Rayeen, A Azeem, A Iqbal, S Payami** - IEEE Transactions on Instrumentation and Measurement, 2024 **Abstract:** The winding inductance of an electric motor is crucial for estimating its performance. In switched reluctance motors (SRMs), this inductance varies with rotor position and phase current, necessitating precise measurement for performance evaluation. This article introduces a sinusoidal excitation methodology for evaluating SRM winding inductance, focusing on measuring inductance profiles across different excitation currents without relying on costly devices like power analyzers, LCR meters, true RMS meters, or specific power supplies, while maintaining high accuracy. A significant challenge in AC methods for inductance measurement is waveform distortion due to core saturation, which reduces accuracy. The proposed method addresses this by using a second-order generalized integrator (SOGI) filter to attenuate distortion-causing frequencies, thereby enhancing solution accuracy in saturation. The magnetizing power component is isolated from the total input power for inductance calculation. Finite element analysis (FEA) of motor winding inductance and performance under both DC and sinusoidal excitation conditions is presented, comparing the analytical model with FEA solutions. Experimental results highlight the effectiveness of proposed method, which delivers precise and comparable outcomes when tested against various methods in the literature and across different excitation currents.
28.	Assessment of electro-thermal runaway dynamics of AC conductor sleeves designed for medium voltage transmission system **R Kumar, CC Reddy** - IEEE Transactions on Dielectrics and Electrical Insulation, 2024 **Abstract:** This paper presents detailed experimental and simulation investigations on the tracking and electro-thermal runaway in overhead conductor sleeves. The 90° and 180° overlapping configurations are extensively studied. The interface tracking inception voltage of the sleeve is experimentally determined under AC voltages for different operating conditions. An experimental setup is proposed to measure the surface and interfacial conductivity. The authors

	present FEM-based simulations to model the sleeve using the measured conductivity, and these simulations are extended until runaway. The results emphasize the effect of overlapping angle on the runaway and tracking. Furthermore, the efficacy of sleeve design is critically evaluated by correlating the simulation results with experimental data and a comparative analysis with covered conductor is also presented. The results offer insights into optimum design of conductor sleeves and are believed to be useful for power utilities.
29.	Assessment of natural radioactivity in the Higher and Tethys Himalayan Rocks along Manali-Leh Highway, India J Yadav, R Beniwal, **PP Singh**, P Singh, R Dalal - Environmental Monitoring and Assessment, 2024 **Abstract:** The Higher and Tethys Himalayan region of NW-Himalaya is less explored from the natural radioactivity mapping assessment, though geologically and tectonically, this region is still active. The concentration of primordial radionuclides (^{226}Ra, ^{232}Th, and ^{40}K) in rock samples of the Manali-Leh Highway region of the Himalayas is determined in the present study using the HPGe detector. The radiological hazard parameters are also estimated in terms of radium equivalent activity (Ra_{eq}), annual effective dose (E_{in} and E_{out}), hazard indices (H_{in}, H_{ex}, H_{α}, and H_{γ}), and gamma absorbed dose rate. SEM–EDS analysis was used to understand the mineralogical composition of the rocks. The activity concentration of ^{226}Ra, ^{232}Th, and ^{40}K radionuclides varies from 1.4 ± 0.9 to 25.3 ± 1.2, 0.7 ± 0.5 to 59.6 ± 1.6, and BDL (below detection limit) to 830.3 ± 45.7 Bq kg^{-1}, with an average value of 13.0 ± 1.0, 21.7 ± 1.0, and 243.7 ± 25.2 Bq kg^{-1}, respectively. The average of Ra_{eq} in the study region lies within the safe limit of 370 Bq kg^{-1}. The hazard indices have values < 1, indicating no radiological hazards to the population from the rocks. The annual effective dose also has values less than the global average value. This study revealed that the rocks of the Higher Himalayan region have a higher concentration of natural radioactivity, while the Tethys Himalayan rocks have lower concentrations of ^{226}Ra, ^{232}Th, and ^{40}K radionuclides. The origin of rocks from different lithologies may be the reason for the natural radioactivity variation. The average concentrations of primordial radionuclides in the region are within the world average indicating that the rocks of the region are safe to be used for different purposes.
30.	Assessment of the evolution of groundwater quality for the state of California, United States using weighted index overlay analysis **A Das, D Banerjee, S Ganguly** - Advances in Geosciences, 2024 **Abstract:** Groundwater serves as a crucial source of drinking water, supports agricultural irrigation, and sustains aquatic ecosystems. However, contamination of groundwater poses significant risks to public health, food security, and ecological balance. Given that groundwater contributes an average of 40 % of California's water supply, ensuring its quality is of paramount importance for the state's municipalities, industries, and agricultural sector. To address this, rigorous groundwater quality assessment and monitoring are imperative to promote sustainable and safe utilization of these resources. Our study leveraged data from the California State Water Resources Control Board (CSWRCB) website, focusing on physiochemical parameters such as total dissolved solids, total hardness, and key cations (e.g., Ca^{2+}, Mg^{2+}, Na^{+} & K^{+}) and anions (e.g., HCO, Cl^{-}, SO & NO). Utilizing the Inverse Distance Weighted (IDW) interpolation method in ArcMap, we generated spatial maps to visualize groundwater quality across California. Furthermore, we applied the Weighted Index Overlay Analysis (WIOA) approach, assigning weights to various physiochemical characteristics based on World Health Organization (WHO) drinking water quality guidelines. Our study aims to facilitate the assessment and monitoring of groundwater contamination in the region, providing valuable insights and formulating a spatial database that can be utilized for effective decision-making and resource management in ArcMap through WIOA analysis.

31.	AviEar: An IoT-based low power solution for acoustic monitoring of Avian Species **R Verma, S Kumar** - IEEE Sensors Journal, 2024 **Abstract:** Birds play a pivotal role in maintaining global biodiversity by serving as vital agents in the key ecosystem functions, such as seed dispersal, insect regulation, and pollination. However, escalating anthropogenic pressures such as deforestation, poaching, and climate change have increasingly imperiled the avian populations worldwide. Consequently, effective monitoring strategies are essential for conservation efforts. However, the traditional monitoring methods often fall short due to limitations in power efficiency and data storage. This paper presents the design and development of AviEar, a novel wireless sensor node tailored for monitoring of avian species. The developed node is an Internet of Things (IoT) device which hosts a MEMS microphone, an ultra-low power ARM Cortex MCU and a storage unit. The proposed system seamlessly integrates acoustic data recording, on-board signal processing, storage, and cloud-based uploads to facilitate remote monitoring. A standout feature is its rapid target species detection algorithm, approximately executing within a mere 1.443 seconds. Without real-time onboard processing, the system would generate redundant data and experience increased battery drain. Its real-time selective logging and transmission framework yields an impressive operational span of up to 2 months at an 8 kHz sampling rate. The field experiments demonstrate AviEar's ability to provide avian acoustic data with 99.6% precision, 95% recall, 97.2% F1-score, a mean 0.77 confidence score, and remarkable power efficiency, showcasing its suitability for sustainable monitoring solutions. Moreover, the outcomes of these deployments furnish conservation decision-makers and researchers with invaluable datasets, empowering them to conduct comprehensive and large-scale monitoring initiatives.
32.	Bayesian neural networks modeling for tool wear prediction in milling Al 6061 T6 under MQL conditions **J Airao, A Gupta, CK Nirala**, AWJ Hsue - The International Journal of Advanced Manufacturing Technology, 2024 **Abstract:** The integration of artificial intelligence, machine learning, and deep learning algorithms into machining processes has made them more intelligent, significantly reducing costs, improving production rates, and enhancing product quality by accurately predicting machining responses. In this study, a Bayesian neural network (BNN) is employed to predict tool wear during the milling of Al6061 T6 alloy, showcasing the novelty of BNN in handling uncertainty and providing reliable predictions. Milling experiments were conducted at three different spindle speeds under dry, flood, and minimum quantity lubrication (MQL) strategies. Machinability was evaluated by considering tool wear, milling forces, and surface quality. Unique to this study is the use of force and current signals as input to the BNN model, capturing real-time data to estimate tool wear. The signals were trained and tested to predict tool wear under varying cutting conditions. The results indicated that tool wear in dry conditions was primarily due to adhesion, leading to higher milling forces and poorer surface quality. In comparison, the wet and MQL conditions resulted in 11–21% and 9–13% less tool wear, respectively, than dry conditions, alongside improved surface roughness and reduced machining forces. The BNN model demonstrated its ability to avoid overfitting, providing highly accurate predictions with an error margin of 2–15% when compared to experimental results. Unlike conventional models, the BNN accounts for prediction uncertainty, making it more robust and reliable across different datasets. Thus, the proposed BNN model proves its effectiveness and generalizability in predicting tool wear under various machining conditions, setting a new benchmark for the application of artificial intelligence in machining processes.
33.	C3E: A framework for chart classification and content extraction **MS Kanroo, HS Kawoosa, K Rana, P Goyal** - Computers and Electrical Engineering, 2025

	Abstract: Incorporating charts into technical documents enhances richness by simplifying complex data representation and improving comprehension. However, automated chart content extraction (CCE) presents a significant challenge within the domain of document analysis and understanding. The CCE problem can be viewed through a series of six sub-tasks: chart classification (CC), text detection and recognition (TDR), text role classification (TRC), axis analysis, legend analysis, and data extraction. Improving these sub-tasks is important for enhancing the effectiveness of CCE. This paper introduces the chart classification and content extraction (C3E) framework, with a primary focus on the first three sub-tasks of CCE: CC, TDR, and TRC. We propose a ChartVision model for the CC, an EfficientNet-based model coupled with a dual-branch architecture incorporating a novel hybrid convolutional and dilated attention module. For text detection and TRC, we introduce a novel CCE method based on YOLOv5, CCE-YOLO, designed for localizing and classifying textual components of varying sizes. Further, for text recognition, we employ a convolutional recurrent neural network with connectionist temporal classification loss. We conducted experimental analysis on benchmark datasets to assess the effectiveness of our approach across each sub-task. Specifically, we evaluated CC, TDR, and TRC methods using the UB-PMC 2020 and UB-PMC 2022 datasets from the ICPR2020 and ICPR2022 CHART-Infographics competitions. The C3E framework achieved notable F1-scores of 94.26%, 92.44%, and 80.64% for CC, TDR, and TRC, respectively on the UB-PMC 2020 dataset and 94.0%, 91.98%, and 84.48% for CC, TDR, and TRC, respectively on the UB-PMC 2022 dataset.
34.	Charge transfer mediated photoluminescence engineering in WS2 monolayers for optoelectronic application B Luhar, **R Dhankhar, RV Nair**… - ACS Applied Nano Materials, 2024 **Abstract:** Optical emissions from two-dimensional transition metal dichalcogenides greatly differ from sample to sample due to their interactions with different substrates with variations in parameters such as the dielectric constant, absorption coefficient, growth conditions, strain, and defects. Often, the mechanisms of environmentally sensitive optical emission in 2D materials are lacking, and it is essential to perform the measurements on the same sample with different substrate backgrounds, which is a challenge. In this work, we explore photoluminescence engineering by comparing the optical properties of WS_2 on SiO_2, TiO_x, and Pt by selectively creating different environments locally on the same sample. The PL-confocal map with good spatial resolution reveals that the emission of WS_2 on TiO_x and Pt is suppressed by charge transfer at the interface. While moving from WS_2 on Pt toward WS_2 on the TiO_x region, a 3-fold enhancement in PL emission has been observed in agreement with a 20% increase in the trion-to-exciton ratio and calculated carrier densities. Further, the transient absorption spectroscopy shows faster exciton recombination in WS_2/Pt (~5.7 ps) and WS_2/TiO_x (~7.2 ps) than WS_2/SiO_2 (~48.5 ps), confirming the charge transfer in varied optical emission of the WS_2 monolayer. Our method paves the way for using charge transfer and controlled carrier injection to design nanoantennas, optoelectronic devices, and quantum optical cavities in 2D materials. 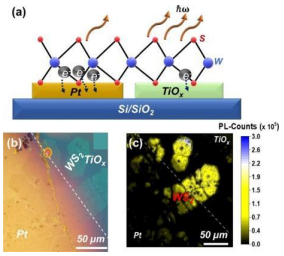
35.	Cold spraying of martensite NAB deposits: a strategy for improved inter-splat bonding **G Vinay, R Kant, H Singh** - Progress in Additive Manufacturing, 2024

	Abstract: Cold spray is a solid-state deposition technique that can be used for both coating and repair applications. Aluminum bronzes are renowned for their excellent corrosion and cavitation resistance in marine environment. Deposition of gas-atomized aluminum bronzes using cold spray is challenging due to the presence of hard martensite. In the present work, gas-atomized nickel aluminum bronze (NAB) powder was heat-treated and segregated according to particle size and subsequently deposited using cold spray. This strategy was successful in enhancing the deposition efficiency (DE) to nearly 100% for the segregated powders from 20% for the as-received powders. Deposition efficiency, hardness, and scratch resistance were used as the parameters to evaluate the inter-splat bonding of the deposits. The bonding state was found to be dependent upon the powder size, as comparatively better properties were achieved for the deposits fabricated with the heat-treated coarser powder.
36.	Conservative deep neural networks for modeling competition of ribosomes with extended length **NK Pande, A Jain, A Kumar, AK Gupta** - Physica D: Nonlinear Phenomena, 2024 **Abstract:** We develop a network model that combines several ribosome flow models with extended objects (RFMEO) competing for the finite pool of ribosomes. This alleviates the need to systematically coarse-grain the mRNA molecules. The dynamics of the network is described by a system of non-linear ordinary differential equations. It is shown that the network always converges to a steady state for a fixed number of ribosomes. Our analysis shows that increasing any of the transition rates along an RFMEO increases its output rate and either the output rates of the other RFMEOs all increase or all decrease. Simulations also demonstrate a counterintuitive result that increasing the ribosomal footprint may sometimes lead to an increase in the network production rate. Next, we propose a conservative deep neural network (CDNN) framework to approximate the solution of the network. The proposed loss function also incorporates the term satisfying the first integral property of the network. Point-wise comparison of the solutions by CDNN is in good agreement with the Runge–Kutta based numerical solution. Also, the CDNN framework offers a closed-form solution of the RFMEONP as a function of free parameters, thus allowing evaluation of the solution at any parameter value without again simulating the system.
37.	Designing lotus-like superhydrophobic self-cleaning surface using carbon nanotubes **S Rahal**, MD Choudhury, SK Das, **D Samanta, PK Agnihotri** - Physics of Fluids, 2024 **Abstract:** Artificial superhydrophobic and self-cleaning surfaces are desirable in many engineering applications. Lotus leaves have long been the benchmark for the design and fabrication of artificial non-wetting surfaces. Here, we report the design and fabrication of superhydrophobic surfaces that mimic the behavior of lotus leaves. Akin to the microstructure of lotus leaves, an intrinsically hierarchical microstructure is created using carbon nanotubes (CNTs). The conventional CNT growth protocol is modified to induce multiscale features with lower diameter CNTs on the top of thicker CNTs. Together they form a dandelion seed head type structure with thicker CNTs such as “beak” and thinner CNTs such as “pappus.” The wetting and self-cleaning behavior of the CNT coated surface is compared with the lotus leaves. The wetting behavior of never-wet commercial spray and Cu and Ni foils are also recorded for comparison. The contact angle, contact angle hysteresis, and sliding angle of water drops on CNT coated surface are comparable with the lotus leaves. The wobbling motion of water drops on the CNT coated surface is similar to that on the lotus leaves and spray coated surface with varying contact line length with time. It also induces the self-cleaning characteristics of CNT coated surfaces similar to lotus leaves. Finally, the present study demonstrates a feasible strategy to design and fabricate lotus leaves like artificial superhydrophobic surfaces with hierarchical CNT structures.
38.	Determining the impact of anthropogenic activities and climate change on landslide susceptibility for the Himalayan region **A Tyagi, N Gupta, RK Tiwari, N James, SR Chavan** - Natural Hazards, 2024

	Abstract: Landslides seriously threaten life and properties in different parts of the Himalayas. The study focuses on deriving the future landslide susceptibility (LS) maps under different climate scenarios for the Himachal Pradesh, India. To accomplish this, first, 15 years landslide database of 267 events was prepared and clustered in three temporal groups (2005–2010, 2010–2015, and 2015–2020). LS maps were prepared for each group by correlating landslides with their causing factors using the artificial neural network (ANN) model. Second, anthropogenic (land use land cover) LULC future projection was simulated using the ANN-based Cellular Automaton model. Third, 2050 projection maps for two climate variables (rainfall and temperature) were prepared by assembling six CMIP6 climate models under four shared socioeconomic pathways (SSPs) scenarios. Fourth, the prepared 2010 and 2015 LS maps, along with projected anthropogenic LULC and climate variables, were incorporated for predicting the future 2050 LS maps. The simulated results show a considerable change in LULC, rainfall, and temperature pattern in the future, which will result in increase of landslides as the forcing situations increase from SSP-1.26 to SSP-5.85. These results can be utilized to revise current land use policies and develop mitigation measures for landslide risk reduction.
39.	Effectiveness of digital screening and brief intervention for alcohol misuse among college students: A state‐wide cluster randomized trial from India A Ghosh…NC Krishnan… **A Kumar… -** Alcohol: Clinical and Experimental Research, 2024 **Abstract:** Background: Alcohol misuse is prevalent among college students globally, including in India. Digital screening and brief interventions (DSBI) promise to address this issue. This study assesses DSBI's effectiveness in a state-wide cluster randomized trial among college students in India. Methods: We recruited 548 participants (274 in each DSBI and digital screening and brief advice-DSBA) from 40 colleges across 10 districts of Punjab, India. Colleges were selected via two-stage cluster random sampling and were allocated to groups using permuted block randomization. Participants with Alcohol Use Disorder Identification Test (AUDIT) scores between 8 and 19 were included. The digital platform directed eligible participants to their respective groups. DSBI participants received information on alcohol harms, normative and personalized feedback, a decisional balance checklist, and a menu of options. DSBA participants received screening and alcohol harm information. Follow-ups were conducted at 3- and 6-month post-intervention. Primary outcome: reduction in AUDIT scores; secondary outcomes: frequency of drinking, drinks per drinking day, and frequency of heavy episodic drinking (HED). Results: Baseline demographics and clinical variables did not significantly differ between groups, except for participants' age. 37.6% were women. Follow-up rates were 513/548 at 3 months and 483/548 at 6 months, with no group differences in attrition. AUDIT scores significantly decreased in both groups at 3 and 6 months (Time $F = 1870.11$, $p < 0.001$, partial $\eta^2 = 0.77$), with no Group × Time effects ($F = 0.160$, $p = 0.85$). Drinking frequency, HED frequency, and drinks per drinking day decreased significantly in both groups without between-group differences. Conclusion: The study highlights the potential policy implications of integrating brief digital interventions for alcohol misuse into educational health initiatives. 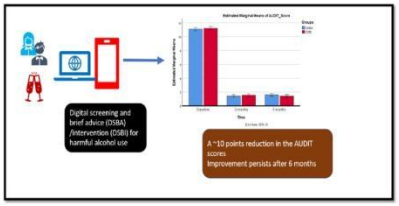
40.	Effects of noise intensity on early warning indicators of thermoacoustic instability: An experimental investigation on a lean-premixed combustion system **N Vishnoi,** R Steinert…**L Kabiraj** - Combustion and Flame, 2025 **Abstract:** In this work, we experimentally investigate the noise-induced dynamics of a lean premixed combustion system operating on natural gas–air mixtures that exhibit thermoacoustic

	instability via a subcritical Hopf bifurcation. The investigation is done before the bistable region with equivalence ratio (ϕ) as the control parameter. We analyze the acoustic pressure oscillations (p') in the combustor and fluctuations in the heat release rate (q') from the laminar quasi-flat flame at increasing levels of white noise. We show the effects of noise intensity on the reliability of various types of early warning indicators (EWIs) to predict the onset of the impending thermoacoustic oscillations. We investigate the indicators based on statistical measures (variance, skewness, and kurtosis), autocorrelation and spectral properties (coherence factor), system identification (growth/decay rates of p'), multi-fractality (Hurst exponent), and time series complexity (permutation entropy and Jensen–Shannon complexity). The coherence factor, variance, and decay rates of p' always increases as the system approaches thermoacoustic instability, indicating their robustness as an EWI under most noise levels. An increase in kurtosis cannot be employed as an EWI. Implementing autocorrelation, skewness, Hurst exponent, permutation entropy and Jensen–Shannon complexity as effective EWIs has limitations: they can be estimated accurately only from pressure oscillations (p') data and work only above a particular threshold value of noise intensity. Our results have direct implication on early prediction and control of thermoacoustic instability in practical gas turbine combustors. Novelty and significance statement: Developing effective early warning indicators (EWIs) to anticipate the onset of thermoacoustic instability is crucial for preventing potential damage and ensuring the reliable operation of lean premixed gas turbine combustion systems. In such systems, inherent noise dynamics undergo variations with changing operating conditions and combustor designs. Specifically, noise intensity increases as the system becomes more turbulent. In this study, we demonstrate that the inherent noise dynamics in a lean premixed combustion system play a crucial role in influencing the trends observed in early warning indicators of thermoacoustic instability. We address several key questions, including (a) whether comparative reliability assessments of different classes of EWIs exist, (b) the effect of variations in noise properties on the efficacy of EWIs, and (c) which EWIs are most reliable considering that noise characteristics depend on the system and may even change with operating conditions within a specific system. This information is critical for engine designers/users, facilitating the development of robust and effective monitoring systems for gas turbine combustion systems.
41.	Efficacy of dynamic eigenvalue in anticipating and distinguishing tipping points K Kulkarni, **S Deb, PS Dutta** - Theoretical Ecology, 2024 **Abstract:** The presence of tipping points in several natural systems necessitates having improved early warning indicators to provide accurate signals of an impending transition to a contrasting state while also detecting the type of transition. Various early warning signals (EWSs) have been devised to forecast the occurrence of tipping points, also called critical transitions. Dynamic eigenvalue (DEV) is a recently proposed EWS that can not only predict the occurrence of a transition but also certain types of accompanying bifurcations. Here, we study the effectiveness and limitations of DEV as an EWS for diverse kinds of critical phenomena. We demonstrate that DEV is a powerful EWS that shows promising results in anticipating catastrophic (first-order or discontinuous) and non-catastrophic (second-order or continuous) transitions in discrete and continuous dynamical systems. However, it falls short in the case of piecewise smooth systems and when the time series data are sparse. Further, the ability of DEV to forecast the type of transition is limited, as it cannot differentiate saddle-node bifurcation from transcritical and pitchfork bifurcations. Despite these limitations, we show that DEV can work as a robust indicator for varying rates at which the transition is approached and with systems involving colored noise.
42.	Electromagnetohydrodynamics (EMHD) of a confined liquid droplet suspended in another liquid pool **P Gupta**, P Dhar, **D Samanta** - International Communications in Heat and Mass Transfer, 2024

	Abstract: The present work investigates, mathematically, the deformation and flow field of a confined leaky dielectric droplet suspended in another liquid pool under steady-state conditions. The physical system is in the presence of an external DC electric field, and the uniform magnetic field. The analysis is within the limitations of small deformation and surface charge convection (Mandal et al., 2014; Bandopadhyay et al., 2016). The approximate analytical solutions are obtained by using various conservation equations along with suitable boundary and interfacial conditions. These equations have been non-dimensionalized and solved using asymptotic expansion to obtain expressions for the deformation and flow fields. Our analysis also shows the effect of confinement, the magnitude of the fields, and their relative orientations on various stress jumps. It also sheds light on the velocities within the droplet and in the surrounding fluid. The droplet deformation is analyzed through the normal stress jump, while the flow field is via the tangential stress jump, along with variations in velocities. Our analysis confirms that when the electric and magnetic forces reinforce each other, deformation will increase, and vice-versa, when they oppose each other. Additionally, denser streamlines are observed in non-zero magnetic field conditions compared to zero magnetic field conditions, suggesting intense fluid mixing for various industrial applications.
43.	EM trigger defender glove: A next-gen IoBT solution for soldier protection **RK Singh, S Mishra** - IEEE Sensors Letters, 2024 **Abstract:** In modern warfare and law enforcement, the Internet of Battlefield Things (IoBT) emerges as a crucial technology offering a paradigm shift in soldier and security personnel safety and threat mitigation. This paper proposes and investigates the development of a groundbreaking system: the EM Defender Glove, aimed at real-time protection against various threats encountered by soldiers, police, and security professionals. Integrating sensors, microcontrollers, and wireless technology, this battery-operated wearable device presents a comprehensive solution to safeguard soldiers, police officers, and security personnel from arms and ammunition misuse and hostile encounters. This novel apparatus utilizes the ability to wirelessly lock/unlock ammunition triggers, incapacitate militants, terrorists, or violent offenders with a potent stun function during one-to-one combat, and disrupt hazardous electronics through Electromagnetic Pulses (EMP). Leveraging long-range Bluetooth Low Energy (BLE), compact yet powerful microcontrollers, and integrated onboard recharging units within the wearable hand glove optimally suits it for practical applications in both battlefield and law enforcement scenarios. Through rigorous design and testing, this study demonstrates the feasibility and effectiveness of the proposed system across various operational environments. The results underscore the significant potential of the EM Defender Glove in enhancing safety and operational effectiveness in both warfare and policing scenarios.
44.	Estimation and validation of snowmelt runoff using degree day method in Northwestern Himalayas Sunita, **V Sood,** S Singh, PK Gupta, HS Gusain, **RK Tiwari**… - Climate, 2024 **Abstract:** The rivers of the Himalayas heavily rely on the abundance of snow, which serves as a vital source of water to South Asian countries. However, its impact on the hydrological system of the region is mainly felt during the spring season. The melting of snow and consequent base flow significantly contribute to the incoming streamflow. This article examines the evaluation of the proportionate contribution to the total streamflow of Beas River up to Pandoh Dam through the snow melt. To analyze the snow melt, the snowmelt runoff model (SRM) has been utilized via dividing the study area into seven different elevation zones within a range of 853–6582 m and computing the percentage of snow cover, ranging from 15% to 90% across the basin. To validate the accuracy of the model, several metrics, such as coefficient of determination (R^2) and volume difference (VD), are utilized. The R^2 reveals that over the span of ten years, the daily discharge simulations exhibited efficiency levels ranging from 0.704 to 0.795, with VD falling within the range of 1.47% to 20.68%. This study has revealed that a significant amount of streamflow

	originates during the summer and monsoon periods, with snowmelt ranging from 10% to 45%. This research provides crucial understanding of the impact of snowmelt on streamflow, supplying essential knowledge on freshwater supply in the area.
45.	Experimental investigation of heat transfer coefficient and frictional pressure drop in flow boiling of R513A: Comparative analysis of micro-fin and smooth tubes NK Vidhyarthi, **S Deb**, S Pal, AK Das - Proceedings of the Institution of Mechanical Engineers, Part E: Journal of Process Mechanical Engineering, 2024 **Abstract:** The heat transfer coefficient (HTC) and frictional pressure drop (FPD) of R513A in flow boiling conditions experimentally investigated in the present article. The study employed micro-fin tubes (MFT1 and MFT2) and smooth tubes (ST1 and ST2) as testing tubes under various operational parameters. The test sections featured standardized tube lengths (1000 mm) and outer diameter (9.52 mm) across all tubes, with variations in mass flux (50–300 $kg \cdot m^{-2} \cdot s^{-1}$), vapor quality (0.02–0.96), saturation temperature (12°C, 17°C, and 22 °C) and heat flux (6, 18, and 30 $kW \cdot m^{-2}$). Research focused on evaluating influence of micro-fin enhancement on flow boiling characteristics, specifically comparing HTC and FPD between micro-fin and smooth tubes. Results indicate significant improvement on HTC within micro-fin tubes compared to smooth tubes, accompanied by reasonable increase in FPD. Additionally, the study validated experimental data against established correlations and conducted sensitivity analysis to understand influence of key parameters on HTC and FPD. Overall, findings contribute valuable insights for optimizing heat exchanger design and thermal system efficiency in flow boiling applications.
46.	Fairness-aware utility maximization for multi-UAV-aided terrestrial networks N Gupta, **S Agarwal**, A Fakhreddine - IEEE Open Journal of Vehicular Technology, 2024 **Abstract:** Integrating unmanned aerial vehicles (UAVs) with terrestrial networks can enable high-speed communication in various applications. UAVs can serve as aerial base stations (ABSs), offering several benefits to the existing terrestrial networks, such as enhanced coverage, increased capacity, rapid deployment, and mobile communication support. However, this integration presents various technical challenges, including coordination, interference management, and dynamic allocation of resources. To address these key challenges, in this paper, we maximize the network utility by jointly optimizing the scheduling and cell association, transmit power of all base stations, and ABS deployment locations in the presence of co-channel interference. A two-stage approach is proposed to obtain a solution. In the first stage, we propose a heuristic solution by using the clustering algorithm to determine the initial ABS locations and user scheduling while ignoring the co-channel interference. In the second stage, we utilize the solution obtained in the first part and develop an interference-aware iterative scheme to jointly optimize user scheduling, resource allocation, and ABS placement. Given the non-convex nature of this problem, we employ the successive convex approximation technique to approximate the non-convex objectives and constraints. Numerical results show the proposed approach's insights and effectiveness over other schemes. Specifically, our proposed approach provides an average of 25% improvement over the benchmark schemes.
47.	First lifetime measurement of the 9^- isomer in ^{92}Nb N Goel, S Nag, B Maheshwari, **D Choudhury**... - The European Physical Journal A, 2024 **Abstract:** A new 9^- isomer has been identified in odd-odd nuclide, ^{92}Nb which was populated using the reaction ^{80}Se(^{18}O, $p5n$)^{92}Nb at a beam energy of 99 MeV. The γ–γ coincidences were measured using Indian National Gamma Array (INGA). The previously reported isomeric state at 11^- was revisited and the half-life is measured to be 103.6(32) ns. The half-life of the newly observed 9^- isomer in ^{92}Nb has been measured to be 35.8(23) ns for the first time. The transition probability B(E2) has been determined for the isomeric state. The isomeric structure has been

	interpreted as a four-quasiparticle excitation, consisting of three protons and one neutron, using large-scale shell model calculations.
48.	Hemodynamics past a dysfunctional bileaflet mechanical heart valve **A Chauhan, C Sasmal** - International Journal of Engineering Science, 2024 **Abstract:** A mechanical heart valve, an essential prosthetic for managing valvular heart disease, consists of a metal frame housing two or three leaflets (depending on the design) that control blood flow within the heart. However, leaflet dysfunction can impede their movement, leading to valve defects. This study extensively investigates the hemodynamics of such a bileaflet mechanical heart valve with dysfunctions of various extents with the help of direct numerical simulations (DNS) under both steady inflow and pulsatile flow conditions. The results are presented and discussed in terms of spatial variations of velocity magnitude, Reynolds stresses, and surface and time-averaged clinically important parameters such as wall shear stress (WSS), pressure drop, and blood damage. Under steady inflow conditions, the flow field becomes unsteady and turbulent even at a modest Reynolds number of 750 when the valve has 50% defective conditions, in contrast to a steady and laminar flow for a fully functional heart valve with 0% defect condition. The values of WSS also increase by around 50%, and net pressure drops by more than 200% with these defective conditions, which further increase as the defective condition increases. On the other hand, the same trend is also seen under pulsatile flow conditions, with maximum values of wall shear stress and blood damage seen during the peak systolic stage of the cardiac cycle, increasing by more than 200% as the defect condition increases from 0% to 50% for the latter parameter. Furthermore, the present study also investigates the effect of blood rheological behaviors such as shear-thinning and yield stress on hemodynamics past this dysfunctional heart valve. It is seen that blood rheological behavior has a substantial influence on hemodynamics at low Reynolds numbers, diminishing as the Reynolds number increases. Under pulsatile flow conditions, blood exhibiting non-Newtonian characteristics such as shear-thinning shows higher values of wall shear stress and blood damage values compared to Newtonian ones. Therefore, the present study highlights the importance of accounting for blood rheology in clinical assessments. However, this study simulates the cases where both valve leaflets are fixed in position, thereby excluding fluid–structure interaction (FSI) from the present simulations. Such conditions are representative of common occurrences in dysfunctional heart valves. All in all, the in-depth analysis and information obtained from this study are expected to facilitate early detection of valve leaflet dysfunction, thereby contributing to improved clinical management of patients with valvular heart disease.
49.	Highly efficient Ru-decorated CeO_2 for photocatalytic hydrogenation and cyclization of levulinic acid to γ-valerolactone **GS More**, R Bal, **R Srivastava** - Sustainable Energy & Fuels, 2024 **Abstract:** The photocatalytic biomass transformation into valuable chemicals and fuels is interesting but challenging. The levulinic acid (LA) to γ-valerolactone (GVL) transformation has been explored under conventional thermal conditions. Reports on the photocatalytic hydrogenation of LA to GVL are rare, obtaining comprehensive information on the complete reduction process is challenging. Herein, CeO_2 was synthesized *via* the hydrothermal method and decorated with varying wt% of Ru to form Ru/CeO_2. The physical characteristics of the catalysts were confirmed through PXRD, TEM, and XPS analyses. The light absorption capacity of CeO_2 and Ru-decorated CeO_2 (specifically 0.5Ru/CeO_2 and 1Ru/CeO_2) was characterized using UV-visible spectroscopy. Additionally, the band structure of CeO_2 and 1Ru/CeO_2 was examined using VB-XPS and UPS analysis. Decorating CeO_2 with Ru improved charge separation and enhanced visible light absorption capacity. The visible light active 1Ru/CeO_2 catalyst achieved ~99% conversion of LA to GVL under 15 W blue LED illumination at 0.2 MPa hydrogen. A mechanistic investigation through control experiments revealed that electrons facilitated the

	reduction of the ketonic group, while C–O cleavage in the acidic group (–COOH) is by the holes, which forms a carbonyl cation or radical, followed by immediate cyclization to GVL. The findings elucidate the active sites and demonstrate the recyclability of 1Ru/CeO_2 for selective LA hydrogenation under visible light. The work is significant from a sustainable chemistry perspective and crucial for the sustainable production of valuable chemicals. 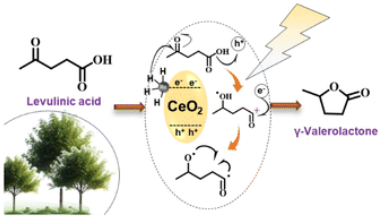
50.	Highly reflective ZrC-Cu-based metal matrix composite coatings deposited via cold-spray for laser protection applications **SW Khan, A Anupam, E Singla, H Singh** - Optics & Laser Technology, 2025 **Abstract:** Lasers are very powerful and can produce high temperatures, capable of melting materials when projected with an appropriate power, exposure time, distance, and beam width. High energy lasers are used for attacking enemy aircraft and missiles; however, the same threat is inevitable to the allied aircraft and missiles. Surface coatings have proven to be a viable solution to reduce damage from such laser attacks. In the present work, ZrC-Cu-based highly reflective coatings were deposited on Al-6061 alloy using the cold spray to develop laser damage resistance. Microstructural characterization, XRD, micro-hardness, reflectivity measurements, and laser ablation tests were conducted on the developed materials. The results showed improved ceramic retention and mechanical properties along with minimal porosity in the coating with increasing ZrC content in the feedstock. Additionally, the XRD analysis revealed that Cu-ZrC composite coatings could be produced by cold spray, without decarburisation of ZrC or oxidation of Cu. Owing to the exceptional purity in coatings, highly reflective coatings were obtained. At the target wavelength of 1080 nm, Cu-30 %ZrC composition achieved a remarkable reflectivity of 75 % (85 % of bulk copper). The coatings with compositions of Cu-30 %ZrC, Cu-50 %ZrC and Cu-70 %ZrC remained undamaged under laser irradiation, whereas Cu-85 %ZrC exhibited a laser ablation pit. These findings provide valuable insights into developing optimized ZrC-Cu coatings against laser irradiation. 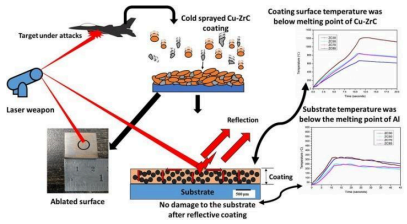
51.	High‐performance alkaline battery‐supercapacitor hybrid based on bimetallic phosphide/phosphate **M Singh, N Thakur, TC Nagaiah** - Advanced Sustainable Systems, 2024 **Abstract:** Transition metal-based materials explored for energy storage applications viz. batteries, supercapacitors and more recently battery-supercapacitor hybrids (BSHs) abundantly involve Co-based materials. However, the supply chain issues and low electronic conductivity force us to look for alternative options. In this regard, Co-free binary metal phosphide/phosphate consisting of Ni and V metal (NiVP/Pi) microspheres as the positive electrode of BSH which shows a high specific capacity of 502 C g^{-1} (1004 F g^{-1}) at 2 mV s^{-1} while retaining a high specific capacity of 214 C g^{-1} (428 F g^{-1}) at 12 A g^{-1} is reported. The high electronic conductivity of binary metal phosphide in NiVP/Pi electrode and the rich electrochemical active sites due to

	Ni and V metal centres results in exciting performance. More interestingly, the hybrid device is successfully developed by employing NiVP/Pi as the positive electrode and carbon nanotubes (CNTs) as the negative electrode. The hybrid device (NiVP/Pi//CNT) is able to achieve a maximum energy density of 22.17 Wh kg^{-1} and a power density of 5 kW kg^{-1} with 91.7% capacitance retention after 7500 continuous galvanostatic charge–discharge cycles.
52.	Inelastic scattering of $PO^{\pm}$ by H_2 at interstellar temperatures **P Chahal, A Kushwaha, TJ Dhilip Kumar** - Monthly Notices of the Royal Astronomical Society, 2024 **Abstract:** Phosphorous species are of great interest in interstellar chemistry since they are the basic blocks for building life here on Earth. Modelling the abundance and environment of recently detected PO^+ under non-local thermodynamic equilibrium (LTE) requires rotational spectra of the molecule along with accurate collisional rates with the most abundant species, hydrogen and helium. A new 4D *ab initio* potential energy surface (PES) of $PO^+ – H_2$ collision is calculated using CCSD(T)/CBS(DTQ) methodology considering rigid rotor approximation. The region containing the minima of the PES is augmented using neural networks (NNs) model while very high potentials (>2500 cm^{-1}) and asymptotic region have been approximated using Slater and R^{-4} functions, respectively. The close coupling calculations have been performed using molscat software for both *ortho* and *para*-H_2. The rate coefficients have been reported for transitions j–j′=1–0, 2–1, 3–2, and 5–4 through which PO^+ has been experimentally detected in interstellar medium (ISM). The rate coefficients for even and odd transitions of PO^+ with *para*-H_2 are compared with that of helium and are found to be 1.1–2.0 times higher. For even transitions (Δj=2), the *ortho*-H_2 rates are 10 per cent higher than *para*-H_2 rates. However, the trend reverses in the case of odd transitions (Δj=1) when higher *J* transitions are considered at low temperatures. At higher temperatures, the *ortho* rates cross the *para*-H_2 rates and become larger than the latter. The new rate coefficients with both *ortho* and *para*-H2 will enable accurate modelling of the PO^+ abundance in the ISM under non-LTE conditions.
53.	Investigating the feasibility of agro-waste briquettes as a sustainable energy source in Borno state Nigeria as pathways for post-conflict and instability recovery **SA Waziri**, K Singh, UA Maina… - Discover Sustainability, 2024 **Abstract:** The growing energy demand and lack of access to clean energy sources call for the development of more energy for cooking in households, briquettes produced using agricultural materials and related biomass have the capacity for utilization as an energy source. This study aims to introduce briquettes as an alternative energy source for cooking within conflict-affected communities in Borno State, northeastern Nigeria, where factors relating to the high cost of charcoal, security constraints, and the environmental impact of tree cutting have sparked apprehension and raised concerns. The study demonstrates the likelihood of adopting briquettes as a cooking fuel alternative in communities recovering from insurgency. Using assessment tools such as household surveys, Key Informant Interviews (KIIs), and Focus Group Discussions (FGDs), involving a total of 536 questionnaires administered to respondents; KII was administered to 37 respondents and 9 FGDs with cooperatives and dealers in traditional fuel were conducted. From the results 73% of the community relies on charcoal as their primary fuel source, since the majority (68.7%) appeared to be low-income households, 24.1% reported that the high cost of charcoal is a major hindrance to continued usage. However, despite the communities showing potential in briquettes, only 3.7% are aware of briquettes as an alternative option for cooking energy indicating the adoption of briquettes being low in the region. A situational assessment was carried and sensitization strategies were recommended as means to enhance livelihoods and build resilience within the community.
54.	Investigation of radon and thoron exhalation rates in soils: Manali-Leh highway region of Himalayas

	J Yadav, R Parkash…**PP Singh…** - Journal of Environmental Radioactivity, 2024 **Abstract:** This study analyses the natural radionuclides concentration (^{226}Ra and ^{232}Th) along with the radon and thoron exhalation rates in 50 soil samples collected from the Manali-Leh Highway region of the Himalayas. The specific activity of ^{226}Ra and ^{232}Th radionuclides was determined using a NaI(Tl) detector, revealing that the concentration values of these radionuclides are lower than the global average. The radon and thoron exhalation rates in the soil samples were measured utilizing a SMART RnDuo detector. The radon mass exhalation rates range from 6 to 87 mBq kg^{-1} h^{-1}, with average values of 25 mBq kg^{-1} h^{-1}. The thoron surface exhalation rates vary from 110 to 757 Bq m^{-2} h^{-1}, with a mean value of 385 Bq m^{-2} h^{-1}. Additionally, the emanation coefficient and alpha dose equivalent for radon were calculated and the correlation between parent and daughter radionuclides was also explored.
55.	IoT based integrated sensing and logging solution for cold chain monitoring applications **LK Baghel, R Raina, S Kumar**, L Catarinucci - IEEE Journal of Radio Frequency Identification, 2024 **Abstract:** Effective cold chain management is critical across various sectors to ensure the integrity of temperature-sensitive goods, ranging from pharmaceuticals to perishable produce. A key challenge within this domain is maintaining items within their required temperature range, typically between 2°C to 8°C, to prevent spoilage or loss of effectiveness. This paper introduces a cost-effective, integrated solution that combines sensors, controllers, and memory into a compact, power-efficient, and low-cost commercial Bluetooth-based temperature & humidity data logger. The proposed solution is particularly useful not only in safeguarding food and pharmaceuticals but also plays a crucial role in the specific context of vaccine storage, such as those for COVID-19, which demands rigorous temperature adherence to ensure efficacy during storage and transportation. Unlike existing solutions, the proposed solution is equipped with interactive algorithms that monitor and record real-time temperature & humidity data throughout the distribution chain. It features a groundbreaking seamless data logging capability, allowing for wireless data retrieval via Bluetooth-enabled devices such as mobile phones, computers, or laptops. The development and testing of the proposed solution have been conducted in our laboratory, ensuring end-to-end performance and efficiency that meet the stringent standards set by health organizations, including the World Health Organization (WHO). A comprehensive comparative analysis further validates the proposed design's accuracy, cost-effectiveness, and power efficiency, demonstrating its potential to enhance cold chain management practices universally.
56.	Irida-graphene: A new two-dimensional electrode material for sodium-ion batteries **M Kaur, N Duhan, TJ Dhilip Kumar** - Journal of Energy Storage, 2024 **Abstract:** The effectiveness of the irida-graphene monolayer for ion storage in sodium-ion batteries (SIBs) is evaluated using density functional theory. The nanolayer possesses a stable structure both dynamically and thermally, along with dependable mechanical properties. The density of states and band structure computations confirmed the excellent conductivity of the monolayer. The storage capacity and energy density have been assessed at 1116.7 $mAhg^{-1}$, and 2854.9 $mWhg^{-1}$ respectively, for Na-ion batteries. Additionally, the small energy barrier of 0.079 eV and heightened diffusion rate of 2.83 x 10^{-4} cm^2s^{-1} for Na ions indicate their easy migration across the surface of the nanolayer during the complete cycle. Furthermore, the open circuit voltage obtained 0.15 V for SIBs, is consistent with the commercial design requirements. Based on the theoretical investigation, irida-graphene clearly demonstrates excellent potential as a superior electrode for next-generation SIBs.

	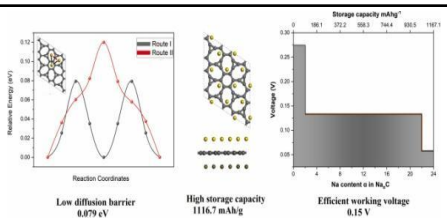
57.	Köthe Amalgams: The ideal type of infinite direct sums **MA Bhat**, P Kolwicz, **GSR Kosuru** - Bulletin of the Malaysian Mathematical Sciences Society, 2025 **Abstract:** We study a special type of infinite direct sums E(X) which can be seen as the amalgam spaces characterized by a local component given by a countable family $X=X\alpha_{\alpha\in I}$ of quasi-normed function spaces and by a global component E, which is a quasi-normed sequence space. We characterize some fundamental properties of E(X) such as completeness, Köthe-duality, order continuity and the Fatou property. We also provide its Banach function space characterization. Then, we apply our general results to the appropriate amalgamations of Lorentz (Orlicz) function spaces and Lebesgue sequence spaces. Moreover, for the Lorentz-type amalgams, we derive interpolation results and prove the boundedness of a class of sublinear integral operators whose kernels satisfy a size condition.
58.	Large area, ultrafast, suppressed dark current and high-performance $PtSe_2/MoS_2$ van der Waals heterostructure based visible to NIR broadband photodetector **G Bassi, R Dahiya**, AG Chakkar, P Kumar, **M Kumar** - Applied Surface Science, 2025 **Abstract:** Group-10 transitional metal dichalcogenide, in particular Platinum selenide ($PtSe_2$), have attracted substantial attention owing to its fascinating properties such as high carrier mobility, narrow bandgap, and high stability in contrast to other low bandgap 2D materials. However, in bare $PtSe_2$, high dark current and lower sensitivity restrict to make high-performance broadband photodetector. Herein, a large area and stable $PtSe_2/MoS_2$ heterostructure based photodetector is fabricated which exhibits suppressed dark current and high-performance with broad 400-1200 nm detection, covering visible to near-infrared region (NIR). The $PtSe_2/MoS_2$ heterostructure device exhibits $\sim 10^3$ order reduction in the dark current, high detectivity, and better stable response as compared to its bare $PtSe_2$ device. Moreover, under NIR (900 nm) illumination, the $PtSe_2/MoS_2$ device demonstrates high responsivity of 17.9 AW^{-1} and high specific detectivity of 9.8×10^{12} Jones at a moderate bias of −5V. It exhibits ultra-fast response with rise/ fall time of 103 µs/117 µs corroborating its high performance. To understand the working of $PtSe_2/MoS_2$ photodetector, a detailed carrier transport mechanism is investigated based on the interface. This work provides a facile strategy to fabricate large area, fast response and high-performance broadband photodetector to build future optoelectronic devices. 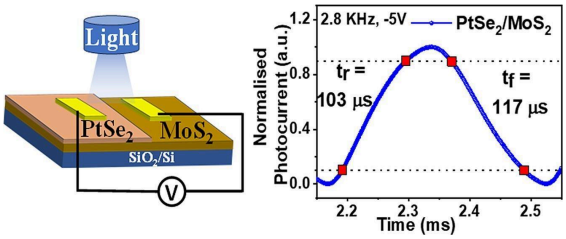
59.	Machine learning driven metal oxide-based portable sensor array for on-site detection and discrimination of mycotoxins in corn sample **Ranbir, G Singh,** N Kaur, **N Singh** - Food Chemistry, 2024

	Abstract: Cereals, grains, and feedstuffs are prone to contamination by fungi during various stages from growth to storage. These fungi may produce harmful mycotoxins impacting food quality and safety. Thus, the development of quick and reliable methods for on-site application is crucial for ensuring food safety and quality monitoring. Herein, we have developed an efficient sensor array based on hierarchically modified metal oxides with azodye-based metal complexes for on-site detection and segregation of harmful mycotoxins present in corn samples. The functionalized material has been fully characterized utilizing various sophisticated techniques. The sensor array successfully detected and differentiated five different mycotoxins with 100 % efficiency, validated by linear discriminant analysis (LDA) score plots. The limit of detection, as determined from calibration curves, ranges from 0.02 to 0.09 ppm for the respective mycotoxins. Additionally, the sensor array has also demonstrated 100 % accuracy in discriminating binary and ternary ratios of mycotoxins in real sample analyses. 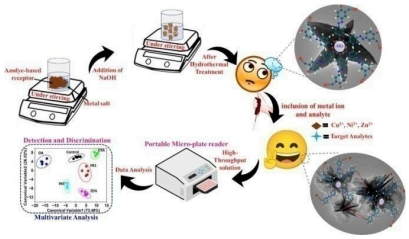
60.	Macrophage foam cell-derived mediator promotes spontaneous fat lipolysis in atherosclerosis models D Banerjee, **D Patra**…**D Pal…** - Journal of Leukocyte Biology, 2024 **Abstract:** Ectopic lipid accumulation in macrophages is responsible for the formation of macrophage foam cells (MFCs) which are involved in the crosstalk with the perivascular adipose tissue (PVAT) of the vascular wall that plays a pivotal role in the progression of atherosclerosis. However, the interrelationship between MFCs and PVAT implementing adipocyte dysfunction during atherosclerosis has not yet been established. We hypothesized that MFC-secreted mediator(s) is causally linked with PVAT dysfunction and the succession of atherosclerosis. To test this hypothesis, MFCs were cocultured with adipocytes, or the conditional media of MFCs (MFC-CM) were exposed to adipocytes and found a significant induction of fat lipolysis in adipocytes. The molecular filtration followed by the high-performance liquid chromatography (HPLC) fractionation and liquid chromatography-mass spectrometry/mass spectrometry (LC–MS/MS) analysis of MFC-CM revealed a novel mediator fetuin-A (FetA) that significantly augments toll-like receptor 4 (TLR4)-dependent fat lipolysis in adipocytes. Mechanistically, MFC-derived FetA markedly increased TLR4-dependent c-Jun N-terminal kinases (JNK)/extracellular signal-regulated kinases (ERK) activation that causes spontaneous fat lipolysis implementing adipocyte dysfunction. Thus, the present study provides the first evidence of MFC-derived FetA that induces adipocyte dysfunction by the stimulation of spontaneous fat lipolysis. Therefore, targeting the crosstalk between MFCs and adipocytes could be a newer approach to counter the progression of atherosclerosis.
61.	Modulating core polarity in metal‐free covalent organic frameworks for selective electrocatalytic hydrogen peroxide production **S Mehta**, N Elmerhi, **S Kaur**, AK Mohammed, **TC Nagaiah**… - Angewandte Chemie, 2024 **Abstract:** Tuning the charge density at the active site to balance the adsorption ability and reactivity of oxygen is extremely significant for driving a two-electron oxygen reduction reaction (ORR) to produce hydrogen peroxide (H_2O_2). Herein, we have highlighted the influence of intermolecular polarity in covalent organic frameworks (COFs) on the efficiency and selectivity of electrochemical H_2O_2 production. Different C3 symmetric building blocks have been utilized to regulate the charge density at the active sites. The benzene-cored COF, which exhibits reduced

	polarity than the triazine-cored COF, displayed enhanced performance in H_2O_2 production, achieving 93.1 % selectivity for H_2O_2 at 0.4 V with almost two-electron transfer and a faradaic efficiency of 90.5 %. *In-situ* electrochemical Raman spectroscopy and scanning electrochemical microscopy (SECM) were employed to confirm H_2O_2 generation and analyze spatial reactivity patterns. These techniques provided detailed insights into localized catalytic behavior, emphasizing the influence of core polarity. 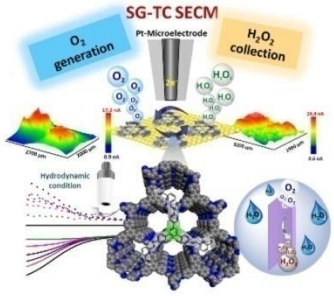
62.	More on the complexity of defensive domination in graphs MA Henning, **A Pandey,** V Tripathi - Discrete Applied Mathematics, 2025 **Abstract:** In a graph G=(V,E), a non-empty set A of k distinct vertices, is called a k-*attack* on G. The vertices in the set A are considered to be *under attack*. A set D⊆V can defend or counter the attack A on G if there exists a one-to-one function f:A↦D, such that either f(u)=u or there is an edge between u, and its image f(u), in G. A set D is called a k-*defensive dominating set* if it defends against any k-attack on G. Given a graph G=(V,E), the minimum k-defensive domination problem requires us to compute a minimum cardinality k-defensive dominating set of G. When k is not fixed, it is co-NP-hard to decide if D⊆V is a k-defensive dominating set. However, when k is fixed, the decision version of the problem is NP-complete for general graphs. On the positive side, the problem can be solved in linear time when restricted to paths, cycles, co-chain, and threshold graphs for any k. This paper mainly focuses on the problem when k>0 is fixed. We prove that the decision version of the problem remains NP-complete for bipartite graphs; this answers a question asked by Ekim et al. (Discrete Math. 343 (2) (2020)). We establish a lower and upper bound on the approximation ratio for the problem. Further, we show that the minimum k-defensive domination problem is APX-complete for bounded degree graphs. On the positive side, we show that the problem is efficiently solvable for complete bipartite graphs for any k>0. Towards the end, we study a relationship between the defensive domination number and another well-studied domination parameter.
63.	Natural radioactivity in rocks and soil along Manali-Leh highway: comparative analysis J Yadav, B Khyalia…**PP Singh**… - Journal of Radioanalytical and Nuclear Chemistry, 2024 **Abstract:** This study compares the concentration of naturally occurring radionuclides in rocks and soil samples taken along the Manali-Leh highway from the Higher and Tethyn Himalayas. The activity of ^{226}Ra, ^{232}Th, and ^{40}K in soil and rock samples was measured using an HPGe detector. The activity of these primordial radionuclides in soil and rocks differs considerably due to variations in geological and tectonic formations in the region. After a particular location, a significant decrease in radioactivity concentration in rocks and soil was also observed.
64.	Nucleophilic ring opening of donor-acceptor cyclopropanes through umpolung reactivity of organochlorophosphines: Phosphine oxide-functionalized boron-pendanted compounds **B Gopal, M Lamba, A Kushwaha, PR Singh, TJ Dhilip Kumar, A Goswami** - Organic Letters, 2024 **Abstract:** We present a novel set of frustrated Lewis pair (FLP) systems that exhibit a remarkable ability to promote the ring opening of donor–acceptor cyclopropanes (DACs). This

	FLP-promoted protocol offers umpolung reactivity of R^1R^2PCl/CN (R^1, R^2 = aryl, alkyl) toward DACs via nucleophilic ring-opening reactions to provide phosphinated boron-pendanted diester compounds. This novel approach exhibits the dual role of $BF_3{\cdot}OEt_2$ as an activator and a reactant. The resulting compounds were found in both the keto and enol forms, with the majority being in the keto form, according to NMR analysis. The enol form was identified by single-crystal XRD analysis, and DFT calculations indicated that the keto form is more stable than the corresponding enol form. 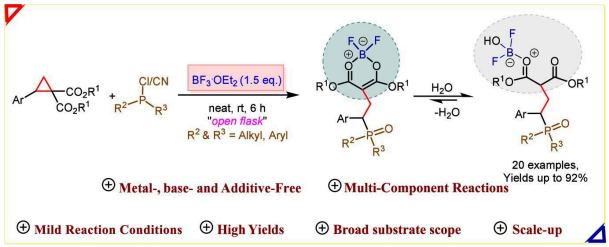
65.	Octa-port dual-polarized antenna/rectenna for MIMO simultaneous wireless information and power transfer (SWIPT) **SK Gupta, A Sharma** - IEEE Microwave and Wireless Technology Letters, 2024 **Abstract:** Wireless sensor networks face a challenge with the limited battery capacity in IoT sensor nodes and low communication quality, hindering network sustainability and increasing maintenance costs. To simultaneously address these issues, a novel octa-port antenna/rectenna with dual-polarization capabilities is proposed for simultaneous wireless information and power transfer (SWIPT) operation. The four ports of the design realize a rectenna for wireless power transfer (WPT), and the other four ports are dedicated to MIMO operation for wireless information transfer (WIT). The rectenna has a gain of 7.2 dBi with a dc beamwidth of 72.2°. The rectenna achieves a good PCE of 50.92% at 1700Ω, translating to a dc power harvesting capacity of 72.47μ W at -8.46 -dBm RF input power. The MIMO antennas maintain a bandwidth of 200 MHz, with S_{11} less than -10 dB centered around 5.8 GHz. The mutual coupling between co-polarized antenna/rectenna ports and among the MIMO antenna ports is less than -12 and -25 dB, respectively.
66.	Optimizing numerical performance of enzymatic coagulation models: Insight into proteolysis and gelation dynamics Z Ansari, M Rae**, J Kumar**, M Singh - Physics of Fluids, 2024 **Abstract:** Cheese manufacturing from milk is a meticulous process that transforms casein micelles into various cheeses through enzymatic action and controlled steps. During enzymatic milk coagulation, three key processes occur: enzymatic proteolysis, coagulation, and gelation. Enzymatic proteolysis breaks down milk proteins, leading to coagulation, where the milk thickens. Gelation then forms a gel-like structure that separates curds from whey, essential for cheese production. To model the enzymatic coagulation of milk, a new mathematical framework is derived based on the conservative formulation of the coagulation equation. To solve this nonlinear complex model, an efficient numerical approach utilizing the finite volume scheme is developed. This method features a straightforward mathematical formulation and robustness for implementation on both uniform and nonuniform grids, enhancing its applicability across various scenarios compared to existing approaches [M. Tsagkaridis *et al.*, "Analysis of turbulent coagulation in a jet with discretised population balance and DNS," J. Fluid Mech. 937, A25 (2022)]. We also discuss the stability condition for the time step to ensure a positive solution. The validation of this new approach involves analyzing number density functions and their integral moments for different gelling and non-gelling kernels. Results indicate that the method captures zeroth and first-order moments with high precision while also computing second-order moments and average micelle sizes formed in the system. Additionally, the impact of the proteolysis constant on gelation is thoroughly examined. This comprehensive capability and

	detailed analysis provide deeper insight into the enzymatic coagulation process, facilitating its efficient optimization.
67.	Optimizing UAV-based data collection in IoT networks with dynamic service time and buffer-aware trajectory planning M Donipati, A Jaiswal, A Hazra, N Mazumdar, **J Singh** - IEEE Transactions on Network and Service Management, 2024 **Abstract:** Unmanned Aerial Vehicles (UAVs) have become vital tools for data collection in Internet of Things (IoT) networks, enabling efficient monitoring and information acquisition across various domains. However, UAV-assisted IoT networks often face significant challenges such as high data loss, latency, and resource inefficiency due to inadequate buffer management and dynamic service time (DST) allocation for IoT nodes. Existing approaches frequently overlook critical factors such as IoT nodes' energy levels, UAVs' energy constraints, and the dynamic data generation rates of IoT devices. To address these challenges, this article introduces a novel strategy for dynamically optimizing UAV trajectories by integrating real-time data from ground nodes and UAV energy levels. Given the DST and buffer constraints (BC) of IoT devices, optimizing UAV trajectories for data collection is a complex problem. We propose an optimization framework that strategically plans UAV trajectories to minimize service time at designated Rendezvous Points (RPs) and bypasses RPs when necessary to reduce the overall trajectory path, taking into account buffer status and dynamic service time adjustments. To efficiently solve this optimization problem, we employ a meta-heuristic technique known as Path Cheapest Arc with Guided Local Search (PCA-GLS) for UAV route planning within predefined time windows. Extensive simulations demonstrate the effectiveness of our proposed solution in optimizing UAV trajectories and improving data collection performance compared to existing algorithms such as BA-UAV, ACO-MS, and NSGA-II.
68.	Oxidative cleavage of α‐O‐4, β‐O‐4, and 4‐O‐5 linkages in lignin model compounds over P, N co‐doped carbon catalyst: A metal‐free approach **A Chauhan, D Rajendra Kanchan, A Banerjee, R Srivastava** - ChemSusChem, 2024 **Abstract:** Developing efficient metal‐free catalysts for lignin valorization is essential but challenging. In this study, a cost‐effective strategy is employed to synthesize a P, N co‐doped carbon catalyst through hydrothermal and carbonization processes. This catalyst effectively cleaved α‐O‐4, β‐O‐4, and 4‐O‐5 lignin linkages, as demonstrated with model compounds. Various catalysts were prepared at different carbonization temperatures and thoroughly characterized using techniques such as XRD, RAMAN, FTIR, XPS, NH_3‐TPD, and HRTEM. Attributed to higher acidity, the P_5NC‐500 catalyst exhibited the best catalytic activity, employing H_2O_2 as the oxidant in water. Additionally, this metal‐free technique efficiently converted simulated lignin bio‐oil, containing all three linkages, into valuable monomers. Density Functional Theory calculations provided insight into the reaction mechanism, suggesting substrate and oxidant activation by P−O−H sites in the P_5NC‐500, and by N−C−O−H in the CN catalyst. Moreover, the catalyst′s recyclability and water utilization enhance its environmental compatibility, offering a highly sustainable approach to lignin valorization with potential applications in various industries.
69.	Pd nanoparticles decorated CeZrOx for enhanced photocatalytic hydrogenation of biomass‐derived compounds **GS More**, R Bal, **R Srivastava** - ChemCatChem, 2024 **Abstract:** The photocatalytic conversion of biomass-derived compounds into value-added chemicals presents a promising protocol for the sustainable production of renewable chemicals. Our study explores the hydrogenation of biomass model compounds under visible light illumination. Zr was incorporated into the CeO_2 framework, forming a CeZrOx(1:0.5) solid

	solution, confirmed by powder X-ray diffraction (PXRD) and X-ray photoelectron spectroscopy (XPS) analyses. The light uptake capacity of the CeZrOx solid solution was characterized using UV–visible spectroscopy. Additionally, the band structure of the CeZrOx solid solution was assessed using valance band X-ray photoelectron spectroscopy (VB-XPS) and Ultraviolet photoelectron spectroscopy (UPS) analysis, revealing a Z-Scheme, which was further confirmed by various control experiments. Upon decorating the CeZrOx(1:0.5) solid solution with 1 wt% palladium (Pd), the resulting 1Pd/CeZrOx(1:0.5) composite exhibited improved charge separation and enhanced visible light absorption capacity. This composite achieved ~99% conversion of furfural to tetrahydrofurfuryl alcohol under a 15 W blue LED illumination and 0.2 MPa hydrogen. Similarly, it demonstrated ~99% conversion of benzyl phenyl ether (BPE) to toluene and phenol under a 10 W blue LED illumination. Our findings elucidate the active sites and demonstrate the recyclability of mixed metal oxides for selective furfural hydrogenation and BPE hydrogenolysis under visible light. 
70.	Perceived parenting practices and health-risk behaviours among indian adolescents: the mediating role of emotion-regulation difficulties **P Singh** - Journal of Child and Family Studies, 2024 **Abstract:** Preventing adolescents from engaging in Health-Risk Behaviours (HRBs) requires a comprehensive understanding of the factors linked to HRBs. Factors like dysfunctional parenting practices and emotion regulation difficulties may significantly contribute to the development and persistence of HRBs. However, this association, particularly the mediating effects of emotion-regulation difficulties, has not been extensively investigated among Indian adolescents, as such research has predominantly centred around Western cultures. The current study explored emotion-regulation difficulties as a mediator in the association between perceived parenting practices and HRBs. The sample comprises 723 adolescents (M_{age} = 16.05; Males = 440) selected from various schools in the Punjab state of India. Structural equation modelling using item-parcels and the path analysis tested the stated hypotheses. As hypothesized, difficulties in emotion regulation were found to be a partial mediator of the parenting-HRB relationship. By offering empirical evidence of this mediational mechanism, the study enhances our understanding of how perceived parenting influences adolescent behaviour. Emotion dysregulation may be the underlying factor behind the development and maintenance of HRBs. These insights can guide researchers in designing targeted interventions to address emotion regulation difficulties and, in turn, help reduce HRBs among adolescents.
71.	Performance optimization study on a novel waste heat flow-based wick-finned distillation system for clean and sustainable pure water production **R Goswami, R Das, S Ganguly** - Sustainable Energy Technologies and Assessments, 2024 **Abstract:** In this work, a novel wick and copper-finned distillation system has been developed based on the flow of waste heat from a biomass engine to efficiently produce a large amount of pure water to meet sustainable development goals. In this novel design, six copper-made fins are employed at a specific location on the waste heat pipe to boost the evaporation process, and a double-layer wick is employed over the glass to enhance the condensation process, which collectively leads to improved system performance. The performance optimization of the

	distillation system has been investigated to obtain the maximum mass of distilled water by varying the operating conditions of the input factors. Further, the Box-Behnken Design, Analysis of Variance, and Regression methods are applied to develop the empirical correlations between the input factors and a response parameter. The effects of various input factors on the response parameter are studied by response surface analysis through surface and contour plots. The experimental results revealed that the maximum value of the mass of the distilled water is obtained as 2.407 kg during 100 min of run at 321 °C of waste heat inlet temperature, 45° of glass angle, and 0.08 m of basin water height. Employing wick and copper fins in the distillation system has positively affected the yield of distilled water productionand increases the output from 2.054 kg to 2.407 kg with a 17.18 % improvement at the optimal conditions. It has been suggested that the highest waste heat inlet temperature level needs to be preferred to produce a large amount of distilled water. In contrast, the moderate levels of glass angle and basin water height provide the maximum output. The quadratic correlation is found to be in good agreement with the experimental values, with a maximum error of 12.03 %. The production cost of distilled water from the present system is found to be 1.91 INR/kg (0.023 USD/kg) through economic analysis. 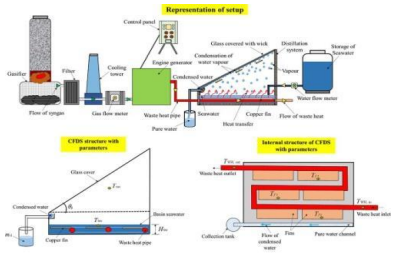 Fig. Schematic of the experimental setup displaying various parts and parameters
72.	Peroxisomes and PPARs: Emerging role as master regulators of cancer metabolism AM Pratama , **M Sharma** , **S Naidu…** - Molecular Metabolism, 2024 **Abstract:** Cancer is a disease characterized by the acquisition of a multitude of unique traits. It has long been understood that cancer cells divert significantly from normal cell metabolism. The most obvious of metabolic changes is that cancer cells strongly rely on glucose conversion by aerobic glycolysis. In addition, they also regularly develop mechanisms to use lipids and fatty acids for their energy needs. Peroxisomes lie central to these adaptive changes of lipid metabolism. Peroxisomes are metabolic organelles that take part in over 50 enzymatic reactions crucial for cellular functioning. Thus, they are essential for an effective and comprehensive use of lipids' energy supplied to cells. Cancer cells display a substantial increase in the biogenesis of peroxisomes and an increased expression of proteins necessary for the enzymatic functions provided by peroxisomes. Moreover, the enzymatic conversion of FAs in peroxisomes is a significant source of reactive oxygen and nitrogen species (ROS/RNS) that strongly impact cancer malignancy. Important regulators in peroxisomal FA oxidation and ROS/RNS generation are the transcription factors of the peroxisome proliferator-activated receptor (PPAR) family. This review describes the metabolic changes in tumorigenesis and cancer progression influenced by peroxisomes. We will highlight the ambivalent role that peroxisomes and PPARs play in the different stages of tumor development and summarize our current understanding of how to capitalize on the comprehension of peroxisomal biology for cancer treatment.
73.	Pyrene functionalized organic receptor-based "Turn-On" fluorescence approach for monitoring of chlorpyrifos in food, soil, and water samples **M Kumar, A Dhiman,** G Singh, N Kaur, **N Singh** - Analytica Chimica Acta, 2024

	Abstract: Background: The unregulated use of pesticides by farmers, for crop productivity results in widespread contamination of organophosphates in real environmental samples, which is a growing societal concern about their potential health effects. The conventional approaches for the monitoring these organophosphate-based pesticides which include immunoassays, electrochemical methods, immunosensors, various chromatography techniques, along with some spectroscopic methods, are either costly, sophisticated, or involves the use of different metal complexes. Therefore, there is an urgent need for sensitive, quick, and easy-to-use detection techniques for the screening of widely used organophosphate-based pesticides. Results: Herein, we demonstrates the metal-free detection of CPF pesticide in aqueous medium, based on the organic nanoparticles of benzimidazole-based cationic receptor (**R1**-ONPs), and thoroughly analyzed using advanced techniques such as AFM, FESEM, and DLS etc. The photophysical investigations revealed that developed **R1**-ONPs exhibited high selectivity towards chlorpyrifos with an enhancement in fluorescence emission. Further, the observed pyrene excimer-based "turn-on" fluorescence mechanism, and the interaction between developed sensor and chlorpyrifos has been validated utilizing ^{1}H, and ^{31}P NMR spectroscopy. The developed sensor can effectively quantify chlorpyrifos up to a detection limit of 18.9 nM (3σ method) with a range of 0–120 μM as well as below the cutoff limit set by FAO. Moreover, the real-time application of developed sensor (**R1**-ONPs) was evaluated to monitor chlorpyrifos in spiked food, water, and soil samples with good (%) recovery. Significance: The development of metal-free, pyrene-excimer-based "Turn-On" fluorescent sensor offers a novel, eco-friendly strategy for the detection of chlorpyrifos in aqueous medium. Additionally, its ability to quantify the chlorpyrifos at levels as low as those set by FAO makes it more efficient tool for monitoring the environmental toxicity ensuring better protection for human, and animal health. 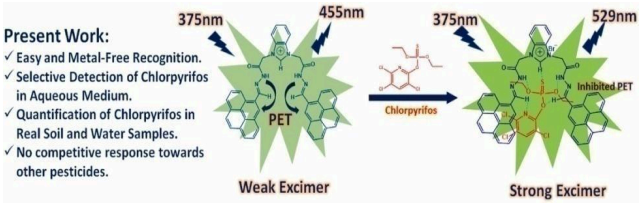
74.	Quantum rectification based on room temperature multidirectional nonlinearity in Bi2Te3 D Kumar, **R Sharma**, F Wang… - Nano Letters, 2024 **Abstract:** Recent interest in quantum nonlinearity has spurred the development of rectifiers for harvesting energy from ambient radiofrequency waves. However, these rectifiers face efficiency and bandwidth limitations at room temperature. We address these challenges by exploring Bi_2Te_3, a time-reversal symmetric topological quantum material. Bi_2Te_3 exhibits robust room temperature second-order voltage generation in both the longitudinal and transverse directions. We harness these coexisting nonlinearities to design a multidirectional quantum rectifier that can simultaneously extract energy from various components of an input signal. We demonstrate the efficacy of Bi_2Te_3-based rectifiers across a broad frequency range, spanning from existing Wi-Fi bands (2.45 GHz) to frequencies relevant to next-generation 5G technology (27.4 GHz). Our Bi_2Te_3-based rectifier surpasses previous limitations by achieving a high rectification efficiency and operational frequency, alongside a low operational threshold and broadband functionality. These findings enable practical topological quantum rectifiers for high-frequency electronics and energy conversion, advancing wireless energy harvesting for next-generation communication.

	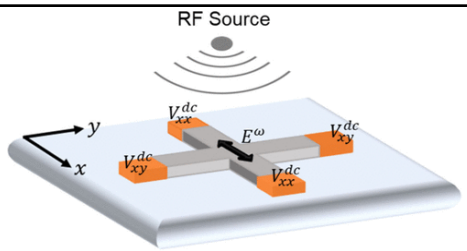
75.	Quantum rotational dynamics of linear C5 at low interstellar temperatures for H2 collision **P Chahal, A Kushwaha, TJ Dhilip Kumar** - The Journal of Chemical Physics, 2024 **Abstract:** The quantum dynamics of carbon chains through H_2 and He collisions in the interstellar medium (ISM) is an important step toward accurate modeling of their abundance in non-local thermodynamic equilibrium conditions. The C_5 ($\Sigma g+1$) molecule is the longest pure carbon chain detected in the ISM to date. While He collisions are computationally easy to perform, the collision with much more abundant H_2 is both complicated and computationally demanding. Using templates for approximating *p*-H_2 collisional rates, such as scaling He rates and using a reduced 4D → 2D potential energy surface (PES), has limited applicability. On the other hand, any such approximation does not exist for *o*-H_2. Therefore, a full rotational dynamics of C_5 with both *p*- and *o*-H_2 is performed considering both molecules as rigid-rotors. The PES is calculated using CCSD(T)-F12a/AVTZ, and a neural network fitting model has been carefully chosen to strictly obey spectroscopic accuracy and augment the PES. The augmented PES is then expanded into radial terms using the bispherical harmonics function, and close coupling calculations have been done to get the cross sections and, subsequently, rate coefficients for various rotational transitions of C_5.
76.	Redox-mediated synthesis of Cu2O/CuO/Mn3O4/C quaternary nanocomposites as an efficient electrode material for oxygen reduction reaction and supercapacitor application A Sharma, YN Banothu, P Majee, S Kumar, **M Prajapati**, **K Kumar**, M Pradhan - Journal of Physics and Chemistry of Solids, 2025 **Abstract:** Earth-abundant transition metal oxides (TMOs) hold significant promise as electroactive materials in various electrochemical energy conversion and storage applications, offering economic and environmental advantages over their less abundant counterparts. In this work, a simple and cost-effective redox-mediated reaction strategy under hydrothermal conditions has been adopted to synthesize the quaternary nanocomposites $Cu_2O/CuO/Mn_3O_4/C$ with variable amounts of carbon. The synthesized nanocomposites have been characterized using various analysis techniques, including powder X-ray diffraction (PXRD), field emission scanning electron microscopy (FESEM), high-resolution transmission electron microscopy (HRTEM), X-ray photoelectron spectroscopy (XPS), Fourier transform infrared spectroscopy (FTIR) and Brunauer–Emmett–Teller (BET). The synthesized COM5 nanocomposite ($Cu_2O/CuO/Mn_3O_4$/C-50), when used as an electrocatalyst for the oxygen reduction reaction (ORR), demonstrates a good limiting current density (J_L), half-wave potential ($E_{1/2}$), and onset potential (E_{onset}) of −5.50 mA/cm^2, 0.75 V, and 0.95 V, respectively, as per the polarization curve. The COM5 nanocomposite exhibits a four-electron transfer mechanism, calculated using the Koutecky-Levich (K-L) equation. In an O_2-saturated 0.1M KOH solution, the COM5 nanocomposite has shown a superior relative current durability of 84.46% over 14,000 s compared to the commercially available 10 wt% Pt/C, indicating its potential application in the ORR. However, for supercapacitor applications, the COM3 nanocomposite ($Cu_2O/CuO/Mn_3O_4$/C-20) as active electrode material in galvanic charge-discharge (GCD) study shows superior performance (201 F/g at 1 A/g) compared to the COM2 nanocomposite (117 F/g at 1 A/g) in neutral aqueous electrolyte, possibly due to the lower charge transfer resistance (R_{ct}) of 24.04 Ω compared to COM2 (34.63 Ω). In two-electrode studies, the COM3 nanocomposite exhibits a good energy density of 24.19 Wh/kg at 1 A/g and a 4.7 kW/kg power density at 5 A/g.

	Additionally, the COM3 nanocomposite shows excellent long-term durability (74% capacitance retention) at the current density of 5 A/g for 8000 cycles. The electrochemical findings indicate that the COM3 nanocomposite stands out as a superior electrode material for supercapacitors, while the COM5 nanocomposite proves to be an effective electrocatalyst for the oxygen reduction reaction. 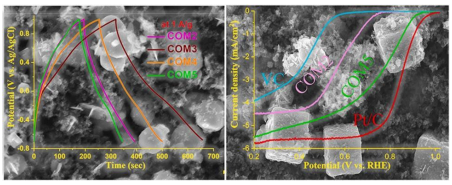
77.	Seasonal refuge patterns of phytoplankton trigger irregular bloom events in a contaminated environment **A Mandal**, S Biswas, PK Tiwari, S Pal - Scientific Reports, 2024 **Abstract:** Several experimental evidences and field data documented that zooplankton may alter its behavioral response in the presence of toxic phytoplankton, reducing its consumption to the point of starvation. This paper is devoted to the mathematical study of such interactions of toxic phytoplankton with grazer zooplankton. The non-toxic phytoplankton is assumed to adopt a density-dependent refuge strategy to avoid over-predation by zooplankton. Both groups of phytoplankton are assumed to suffer direct harm from anthropogenic toxicants, while zooplankton is affected indirectly by ingesting contaminated phytoplankton. We calibrate the proposed model with the field data from Talsari and Digha Mohana, India, and estimate some crucial model parameters consistent with the behavior of the observed data. Our results demonstrate that zooplankton grazing on toxic phytoplankton plays a key role in the emergence or mitigation of plankton blooms. We also highlight the system's potential to exhibit multiple stable configurations under the same ecological conditions. The plankton system experiences significant regime shifts, which are explored through various bifurcation scenarios, such as transcritical and saddle-node bifurcations. These shifts are influenced by changes in refuge capacity, species growth rates, and environmental carrying capacity. Furthermore, we incorporate environmental variations due to seasonal periodic or almost periodic changes, allowing the refuge parameter to be time-dependent. We observe that the forced system exhibits double periodic solutions. Moreover, stronger seasonal variations in the refuge pattern lead to irregular chaotic blooms. In conclusion, the results offer valuable insights into the sustainability of biodiversity, potentially shedding light on the origin of diverse plankton bloom phenomena.
78.	Squeeze film damping due to flexible and rigid body motion in MEMS: a comparison of analytical, numerical and experimental results **S Singh, N Kumar** - Microsystem Technologies, 2024 **Abstract:** In MEMS [Micro Electro Mechanical Systems] based sensors, squeeze film air damping is the dominant mode of energy dissipation. The analytical solutions are mainly limited to simple geometries with rigid-body-movement based squeeze-motion in MEMS, but very less consideration has been given in literature to estimate damping in MEMS structures that involve both flexible and rigid-body movements based squeeze film action. In this paper, the results from analytical and numerical solutions both for rigid-body case and flexible structures are compared. This comparison is done both at low and high squeeze-numbers. Modal-Projection numerical technique that can account the flexible deformation of MEMS structure is discussed and validated using experimental results of a microstructure operated at high squeeze number or high frequency. It is observed that analytical solutions, based on assumption of uniform-squeeze-motion between rigid-parallel-plates, can significantly over estimate the squeeze film parameters for flexible or elastic structure of a MEMS piezoresistive accelerometer.

79.	Suppression and augmentation in vortex shedding frequency due to fluid elasticity **A Chauhan, S Raffi, C Sasmal** - Journal of Non-Newtonian Fluid Mechanics, 2024 **Abstract:** Several previous experimental and numerical studies have demonstrated the suppression of vortex shedding frequency from bluff bodies, such as circular cylinders, due to fluid elasticity induced by adding solid polymer additives to a solvent like water, even in parts per million (ppm) quantities. However, this study reveals a more complex relationship between the two using extensive two-dimensional (2D) direct numerical simulations (DNS) of flows past a circular cylinder at a fixed Reynolds number of 100. Our findings show that the vortex shedding frequency initially decreases with increasing Weissenberg number (a measure of fluid elasticity), reaches a minimum at a critical Weissenberg number, and then increases with further increments in the Weissenberg number. The same non-monotonic trend is also observed in the temporal variation of the spanwise velocity component fluctuation within the flow domain. This study aims to elucidate the reasons behind these non-monotonic trends in vortex shedding frequency and velocity component fluctuations as functions of the Weissenberg number. Our detailed analysis attributes these trends to significant alterations in the vortex-shedding mechanism as fluid elasticity increases due to the appearance of inertio-elastic instability at higher Weissenberg numbers. Our findings also align with limited experimental observations of similar unexpected behaviors in viscoelastic fluids, providing new insights into the underlying mechanisms. Moreover, the study highlights that shear-thinning behavior in viscoelastic fluids counteracts these non-monotonic trends, instead promoting a monotonic increase in vortex shedding frequency with the Weissenberg number. Finally, the 2D simulation results show both qualitative and quantitative agreement with limited three-dimensional (3D) simulations conducted at higher Weissenberg numbers where the flow may transit from 2D to 3D due to the appearance of inertio-elastic instability.
80.	Surface wave scattering on an asymmetric trench **A Aggarwal, SC Martha**, Y Stepanyants - Waves in Random and Complex Media, 2024 **Abstract:** The problem of water wave scattering over an asymmetric trench is investigated. An infinite system of algebraic equations for amplitudes of traveling and evanescent modes is derived and solved using Takano's approach for finding the scattering coefficients, viz., the reflection and transmission coefficients. Within the long-wave approximation, the explicit analytical forms of scattering coefficients are derived. The principal goal of this research is to identify conditions in which an exact standing wave occurs and to investigate behavior of scattering coefficients as functions of asymmetric trench parameters. The characteristics of scattering coefficients are discussed in a comprehensive manner which includes their non-monotonic dependence on depth and width variations. It is shown that the scattering coefficients have oscillating dependence on trench width and some other trench parameters. The conditions on depth ratios, trench width, and frequency parameter needed for the formation of the exact standing wave are found with the help of standing wave ratio. Standing waves can be hazardous for boats traveling over underwater trenches. Additionally, it is found that our numerical results are consistent with the law of energy flux conservation. The results can help marine engineers optimize the underwater trenches to reduce wave impact on the coast.
81.	Synergistic catalysis for promoting selective C-C/C-O cleavage in plastic waste: structure-activity relationship and rational design of heterogeneous catalysts for liquid hydrocarbon production **A Manal, A Shivhare**, S Lande, **R Srivastava** - Chemical Communications, 2024 **Abstract:** Ever-increasing consumption of plastic products and poor waste management infrastructure have resulted in a massive accumulation of plastic waste in environments, causing adverse effects on climate and living organisms. Although contributing ~10% towards the total plastic waste management infrastructure, the chemical recycling of plastic waste is considered a

	viable option to valorize plastic waste into platform chemicals and liquid fuels. Among the various chemical upcycling processes, catalytic hydroprocessing has attracted interest due to its potential to offer higher selectivity than other thermal-based approaches. Heterogeneous catalytic hydroprocessing reactions offer routes for converting plastic waste into essential industrially important molecules. However, the functional group similarities in the plastic polymers frequently constrain reaction selectivity. Therefore, a fundamental understanding of metal selection for targeted bond activation and plastic interaction on solid surfaces is essential for catalyst design and reaction engineering. In this review, we critically assess the structure–activity relationship of catalysts used in the hydroprocessing of plastic waste for the selective production of liquid hydrocarbons. We discuss the significance of C–C/C–O bond activation in plastic waste through active site modulation and surface modification to elucidate reaction networks and pathways for achieving selective bond activation and cleavage. Finally, we highlight current challenges and future opportunities in catalyst design to upcycle real-life plastic waste and produce selective liquid hydrocarbons. 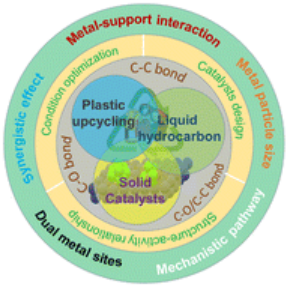
82.	Synergy of nanocrystallinity, temperature, and “the Third Element Effect” for uncommon oxidation resistance of Fe‐Cr‐Al alloys RKS Raman, **R Kumar,** SR Bakshi - Small, 2024 **Abstract:** Nanocrystalline structure, oxidation temperature, and “The Third Element Effect” are among the factors that can profoundly govern the characteristics of the oxide scales that develop on oxidation-resistant alloys, thereby, their synergistic effect can considerably influence alloys’ oxidation kinetics. As a result of the synergy, certain iron-chromium-aluminium (Fe-Cr-Al) alloy showed superior oxidation resistance at 800 °C than at 700 °C (whereas oxidation resistance commonly decreases with the increase in temperature). The superior resistance at higher temperatures is considerably enhanced when the structure of the alloy is nanocrystalline vis-à-vis the common microcrystalline structure. Nanocrystalline alloy oxidizes at a negligible rate (*c.f.*, its microcrystalline counterpart). The characterization of the oxide scale demonstrates that the oxidation temperature governs the formation of the protective oxide scale with/without the assistance of the “Third element Effect”. The findings may potentially have considerable commercial implications.
83.	Syntheses and properties of two isomeric phenanthroacephenanthrylene derivatives **PK Sharma, A Babbar, S Sahewal, S Das** - European Journal of Organic Chemistry, 2024 **Abstract:** Cyclopenta-annulated polycyclic aromatic hydrocarbons (CP-PAHs) are of significant interest due to their unique optoelectronic properties and applications in organic electronic devices. Phenanthroacephenanthrylene (PAP) isomers are CP-PAHs that have been rarely investigated, and only the [9,10-*e*]PAP isomer was explored to date. Herein, we report the syntheses, crystal structure and optoelectronic properties of two PAP isomers, 7-ethoxy[2,1-*e*]PAP 1 and 9-ethoxy[1,2-*e*]PAP 2. The structural isomers were synthesized in multi-steps, and structural elucidations were performed using NMR, mass, and single-crystal X-ray diffraction analyses, revealing planar backbone of the isomers. UV-visible absorption and fluorescence spectra of compound 1 were red-shifted than that of 2, suggesting smaller

	HOMO–LUMO energy gap which is further validated by DFT calculations that suggested the lowering of HOMO–LUMO spacing could be attributed to the greater destabilization of HOMO for 1. 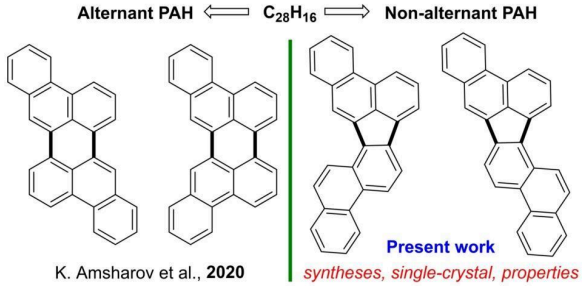
84.	Synthesis of CF3CH2‐amides/propiolamides/acrylamides: The TfOH catalyzed reactions of nitrile compounds with CF3CHN2 **S Devi, M Kumar, M Lamba, A Goswami** - Advanced Synthesis & Catalysis, 2024 **Abstract:** An efficient and operationally simple protocol to access *N*-(2,2,2-trifluoroethyl)amides/propiolamides and acrylamides via direct conversion of easily accessible nitriles (aryl/alkyl/alkynyl/vinyl) and *in situ* generated CF_3CHN_2 as trifluoroethylating reagent has been developed. The protocol offers broad functional group tolerance under mild reaction conditions. Furthermore, the conversion of trifluoroethylated propiolamide into its triazole analog via Ru-catalyzed [3+2] cycloadditions using BnN_3 clearly indicates its versatility in the synthetic applications. 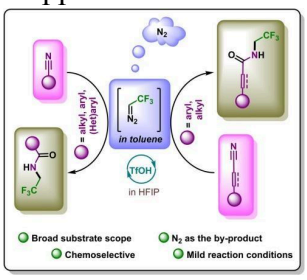
85.	TCAD-based investigation of 1/f noise in advanced 22 nm FDSOI MOSFETs **P Khedgarkar**, M D Ganeriwala, **P Duhan** - Applied Physics Letters, 2024 **Abstract:** In this work, the mechanistic insights behind low-frequency noise (LFN) of the advanced ultrathin body and buried oxide fully depleted silicon-on-insulator based metal–oxide–semiconductor field effect transistor (MOSFET) are unveiled. The gate voltage-induced noise power spectral density (SVG) is inversely proportional to frequency f (i.e., SVG $\propto 1/f^{\gamma}$, $\gamma \sim 1$ is the frequency exponent) for nMOSFET and pMOSFET. Detailed numerical simulations are performed and well calibrated to reported SVG vs f characteristics. Simulation results are consistent with the reported experimental observations. We demonstrate that LFN is caused by the charge carrier number fluctuation mechanism, which is originated by trapping and de-trapping of channel charge carriers via. bulk traps (from oxygen vacancies) in the hafnium dioxide (HfO2) layer, but not through traps at the silicon dioxide (SiO2)/channel interface. This work therefore explains the similar magnitude of SVG in both nMOSFET and pMOSFET observed experimentally and further suggests that oxygen vacancies inside gate oxides are critical to suppress the low-frequency noise in emerging high-k based MOSFETs.
86.	TENDRA: Targeted endurance attack on STT-RAM LLC **P Sinha**, M L Sai, S Das, **VK Tavva** - IEEE Embedded Systems Letters, 2024 **Abstract:** Spin Transfer Torque RAM (STT-RAM) based Last Level Cache (LLC) offers significant benefits like high density and low refresh energy, but faces challenges like high write

	latency and limited endurance. Malicious attacks in a multi-core setup need access to only a single core to perform repeated attacks on specific memory locations that can lead to an accelerated lifetime degradation of the STT-RAM LLC cells. To highlight this vulnerability of STT-RAM LLC we propose two variations of TENDRA (Targeted Endurance Attack), namely, Recurring Location Attack (RLA) and Recurring Toggle Attack (RTA). Our work highlights the efficiency of these attacks on modern counter based wear leveling techniques and also the effect of wear leveling on these attacks.
87.	Tetracycline degradation for wastewater treatment based on ozone nanobubbles advanced oxidation processes (AOPs) – Focus on nanobubbles formation, degradation kinetics, mechanism and effects of water composition **P Koundle, N Nirmalkar,** M Momotko… - Chemical Engineering Journal, 2024 **Abstract:** Presence of pharmaceuticals, especially antibiotics, in industrial and domestic effluents causes serious damage to the environment. Classic wastewater treatment processes, in particular conventional biological treatment methods, are not sufficient to rapidly eliminate antibiotics. Typically, Advanced Oxidation Processes (AOPs) based on activation of hydrogen peroxide, ozone or persulfate for formation of particular type of radical species or singlet oxygen are used. A one of cutting-edge technologies to increase effectiveness of AOPs based on ozone are nanobubbles based processes. Thus, this paper focuses on utilization of ozone in the form of nanobubbles for degradation of tetracycline (TC). The effects of several reaction parameters, such as antibiotic concentration, ozone intake, pH, presence of salts, were investigated. This study revealed that the presence of ozone nanobubbles had a substantial positive impact on the degradation of TC. This improvement may be attributed to the enhanced mass transfer and the production of reactive radicals that occur during the collapse of the nanobubbles. Identification of Reactive Oxygen Species (ROS) revealed a significant contribution of hydroxyl radicals in the degradation of the antibiotic. AOP based on O_3 nanobubbles generated mostly hydroxyl (•OH) and superoxide anion (O_2•$^-$) radicals providing 100 % degradation of 100 mg/L TC within 20 min at 8 mg/L ozone concentration. Based on identified by LC-MS intermediates a detailed degradation mechanism has been described. Degradation of TC and intermediates transformations included methylation, hydroxylation, ring-opening steps as well as cleavage of C-N bonds. This research introduces a novel technique combining nanobubbles with advanced oxidation processes (AOPs), which is anticipated to provide enhanced efficiency and environmental sustainability. 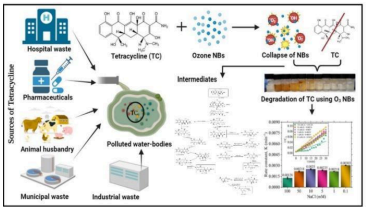
88.	The effect of resummation on retarded Green's function and greybody factor in AdS black holes JB Amado, **S Chakrabortty, A Maurya** - Journal of High Energy Physics, 2024 **Abstract:** We investigate the retarded Green's function and the greybody factor in asymptotically AdS black holes. Using the connection coefficients of the Heun equation, expressed in terms of the Nekrasov-Shatashvili (NS) free energy of an SU(2) supersymmetric gauge theory with four fundamental hypermultiplets, we derive asymptotic expansions for both the retarded Green's function and the greybody factor in the small horizon limit. Furthermore, we compute the corrections to these asymptotic expansions resulting from the resummation procedure of the instanton part of the NS function.

89.	The impact of modulation techniques on brushless DC motor drive D Dwivedi, **S Singh**, **J Kalaiselvi**, KA Chinmaya - International Journal of Circuit Theory and Applications, 2024 **Abstract:** Three-phase brushless DC (BLDC) motors are cost-effective and are increasingly used in various speed control applications. The phase voltage, DC-bus utilization, current ripple, and torque ripple are major performance parameters for a BLDC motor drive. Different pulse width modulation (PWM) methods will diversely influence these parameters. This paper presents the phase voltage, current ripple, and DC-bus utilization analysis of BLDC motor drive for four PWM techniques and provides a comparative analysis. The current ripple of the BLDC drive is evaluated with low and high switching frequency operations. Phase voltage and DC-bus utilization of a BLDC motor are evaluated using analytical methods and validated experimentally. The investigation provided in this work are significant for PWM selection and implementation for low and high switching frequency operations. Both low- and high-frequency operations are performed by supplying the BLDC drive from a silicon carbide (SiC) based inverter. These PWM techniques are also compared, considering high and low-speed applications. Experimental results of SiC inverter-fed BLDC motor drive are provided to substantiate the proposed work.
90.	The multidimensional coagulation and collisional breakage equation with unbounded kernel D Ghosh, DC Chang, **J Kumar,** JC Yao - Applicable Analysis, 2024 **Abstract:** Many scientific and technical fields have benefited from the understanding of the Coagulation and Collisional Breakage Equation (CCBE). In one-dimensional CCBE, only one property of the particle (like size or mass of the particle) is considered. However, there are other factors (like including volume, enthalpy, porosity, mole number, binder content, and more) that affect how particle ensembles behave. Therefore the study of multidimensional CCBE is more accurate. For the multi-dimensional (CCBE), we denote the property characteristics vector as $\vec{x}=(x1,x2,\ldots,xd)\in\mathbb{R}d+$. In this research work, the existence of a continuous solution is investigated where collision rate satisfies $C(\vec{x},\vec{y})\leq c\prod di=1(1+xi)\nu(1+yi)\nu$, where $c>0$ is a constant, $0\leq\nu\leq\theta$ and the coagulation kernel satisfies the following, $K(\vec{x},\vec{y})\leq k\prod di=1(1+xi)\alpha(1+yi)\alpha$, where k is a positive constant, $0\leq\alpha\leq\theta$ and $0<\theta\leq1$. Additionally, the uniqueness of the solution is shown. To prove the result, we have defined a new norm and examined the equicontinuity with respect to time and the property characteristics vector and Arzelà–Ascoli theorem is used.
91.	The role of cartilage tissue engineering in osteoarthritis treatment: The bench to bedside translation **A Mukherjee, S Sarkar, A Poundarik, B Das** - Journal of Polymer Science, 2024 **Abstract:** Cartilage tissue engineering holds huge promise for joint defects and osteoarthritis (OA) conditions which otherwise have limited treatment options due to cartilage's inherent inability to self-repair. Chemical cues play a pivotal role in regulating chondrocyte behavior and matrix synthesis. Strategies utilizing growth factors, small molecules, and biomaterial-based delivery systems aim to modulate chondrogenic differentiation, proliferation, and matrix deposition, while recent insights emphasize the significance of mimicking native tissue gradients for optimal regeneration outcomes. Mechanical stimuli profoundly influence chondrocyte phenotype and function, necessitating precise control of the mechanical microenvironment in tissue engineering strategies. Advances in biomaterial design, scaffold fabrication, and bioreactor systems facilitate the tailored modulation of mechanical cues, including substrate stiffness, topography, and dynamic loading regimes. This review showcases the latest advancements in engineering both the chemical and mechanical microenvironment to enhance chondrocyte regeneration. Furthermore, exploring the synergistic effects of combining chemical and

	mechanical cues underscores the importance of multifaceted approaches in promoting robust chondrocyte regeneration. The review also addresses challenges and future directions in the field, such as achieving spatially organized tissue architecture and integrating patient-specific factors, to propel advancements in cartilage tissue engineering. We also conducted a comprehensive enlistment for the clinical trials and tissue engineering-based marketed products for OA therapy. 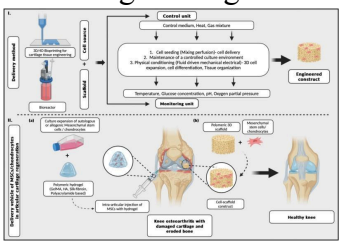
92.	The role of inflammatory cascade and reactive astrogliosis in glial scar formation post-spinal cord injury **M Bhatt, M Sharma, B Das** - Cellular and Molecular Neurobiology, 2024 **Abstract:** Reactive astrogliosis and inflammation are pathologic hallmarks of spinal cord injury. After injury, dysfunction of glial cells (astrocytes) results in glial scar formation, which limits neuronal regeneration. The blood–spinal cord barrier maintains the structural and functional integrity of the spinal cord and does not allow blood vessel components to leak into the spinal cord microenvironment. After the injury, disruption in the spinal cord barrier causes an imbalance of the immunological microenvironment. This triggers the process of neuroinflammation, facilitated by the actions of microglia, neutrophils, glial cells, and cytokines production. Recent work has revealed two phenotypes of astrocytes, A1 and A2, where A2 has a protective type, and A1 releases neurotoxins, further promoting glial scar formation. Here, we first describe the current understanding of the spinal cord microenvironment, both pre-, and post-injury, and the role of different glial cells in the context of spinal cord injury, which forms the essential update on the cellular and molecular events following injury. We aim to explore in-depth signaling pathways and molecular mediators that trigger astrocyte activation and glial scar formation. This review will discuss the activated signaling pathways in astrocytes and other glial cells and their collaborative role in the development of gliosis through inflammatory responses. 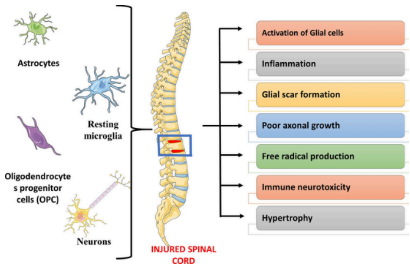
93.	Translating theoretical insights into an emotion regulation flexibility intervention: assessing effectiveness **P Sharma, P Singh** - Cognition and Emotion, 2024 **Abstract:** Objective: Traditional research often categorizes emotion regulation strategies as adaptive or maladaptive, overlooking crucial situational and individual differences that dictate their efficacy. The literature highlights the need for a more nuanced approach, like the role of emotion regulation flexibility. Despite its importance, research on developing and testing interventions that promote this flexibility is scarce. Addressing this gap, our study designed and tested an "Emotion Regulation Flexibility Booster Program" (ERFBP). We aimed to assess its efficacy in improving emotion regulation flexibility (ERF) and its impact on various mental health indicators. Method: We recruited 153 participants with low emotion regulation flexibility,

	randomly assigning them to experimental, control, and no-treatment groups. The experimental group was provided with an intervention based on an ERF model. The control group received sessions on study habits, whereas no-treatment group received no training. Results: The analysis indicated that participants in the ERFBP group exhibited significant changes in ERF, subjective wellbeing, and emotion regulation goals and psychological distress compared to baseline measurements and post-intervention scores of other two groups. Conclusion: These findings support the effectiveness of the ERFBP in enhancing ERF and wellbeing. However, further research must confirm these findings across diverse contexts and populations.
94.	U (VI) mitigation from contaminated groundwater using γ-alumina coated SiC ceramic microporous membrane **M Verma**, N Santra, **VA Loganathan**, N Kayal - Separation and Purification Technology, 2024 **Abstract:** In this study, we have focussed on elucidating uranium adsorption mechanism on to a novel γ-alumina coated SiC ceramic microporous membrane using surface complexation modelling (SCM) approach. The effect of contact time had no impact on U(VI) removal as adsorption by nanoporous γ-alumina was instantaneous, which was also confirmed using batch adsorption kinetic experiments. γ-alumina coated at 4.5 mg cm^{-2} was able to treat 173 L of U(VI) contaminated water having 200 µg of U L^{-1} with 1 m^2 of membrane surface area. Varying the pH of aqueous solution containing U(VI) from pH 4.0 to 10.0 showed significant changes in uranium uptake by the composite membrane with maximum U(VI) removal occurring at pH 5.5. The adsorption mechanism of uranium onto γ-alumina was explained through formation of bidentate surface complexes (i.e. $(>SOH)_2UO_2CO_3^-$, $(>SOH)_2UO_2^+$, and $(>X)_2UO_2$). The results of SCM predicted the batch pH edge experiment within a root mean square error of 0.04. Among various co-ions added along with U(VI), calcium, magnesium, and salinity reduced U(VI) removal whereas phosphate resulted in increased U(VI) removal. The presence of dissolved organic matter (DOM) reduced U(VI) removal due to lack of adsorption between U(VI)-DOM complexes and the membrane surface. 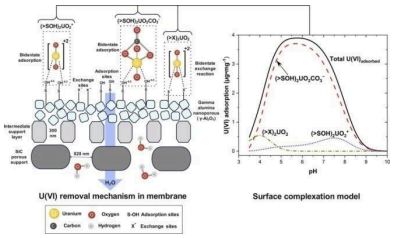
95.	Understanding flow field transitions and vortex dynamics in polymer melts flowing through a microchannel with sidewall cavities **S Gupta, C Sasmal** - Rheologica Acta, 2024 **Abstract:** The flow of polymer melts through microscale systems is crucial in several additive manufacturing processes, such as extrusion, injection molding, and polymer three-dimensional (3D) printing. This study conducts a numerical investigation of the flow dynamics of low-density polyethylene (LDPE) polymer melts through a straight microchannel with sidewall cavities. Specifically, it examines the effects of flow rate (quantified by the Weissenberg number) and sidewall cavity aspect ratio (the ratio of cavity width to height) on the transition of the flow field from steady and laminar to unsteady and chaotic due to elastic instability. The findings indicate that flow field fluctuations in polymer melt flows, induced by elastic instability, increase progressively with the Weissenberg number. However, beyond certain Weissenberg number values, the fluctuation intensity is unexpectedly suppressed, indicating a suppression of elastic instability at high Weissenberg numbers. Additionally, as the cavity aspect ratio increases, the flow field fluctuations increase. Nevertheless, the differences in fluctuation become minimal at high Weissenberg numbers. Not only this non-monotonic transition in the flow field but also the

	vortex dynamics within the system depend strongly on the Weissenberg number and cavity aspect ratio. Various vortices appear in the present flow system, particularly within the cavity region, such as the central primary vortex, corner vortex, and lip vortex. The size, shape, appearance, and disappearance of these vortices are significantly influenced by the Weissenberg number and cavity aspect ratio. Moreover, the study explores the impact of adding another cavity to the microchannel sidewall on this flow transition, and it finds that the additional cavity does not affect the onset of the flow transition. However, it does introduce some differences in vortex dynamics.
96.	Uniform temperature distribution and reduced convection losses: Top and bottom heating strategies for nanofluid and surface absorption-based solar thermal systems **AS Kashyap**, V Bhalla, **H Tyagi** - Applied Thermal Engineering, 2024 **Abstract:** In direct absorption solar collectors (DASC), the suspension of nanoparticles in base fluid increases the solar absorptivity for volumetric absorption, which results in better efficiency when compared to transparent base fluids. However, a temperature gradient exists in the nanofluid volume while irradiated in the gravitational direction which can be diminished by changing the irradiation direction. The irradiation provided from opposite direction to gravity introduces natural convection in nanofluid and maintains a uniform temperature. The novelty of present experimental study is to compare and understand the effect of two directions of irradiation i.e., heating from the top (TH, in the gravitational direction) and heating from the bottom (BH, in the opposite direction of gravity) on both surface absorption-based (SAS) solar collector and volumetric absorption-based (VAS) solar collector. In VAS 6 different mass fractions of carbon-based nanofluids have been used. From the results, it was found that BH gives a higher and uniform temperature rise compared to TH for both the SAS and VAS. For VAS with TH, a maximum temperature rise of 8.51 °C is obtained at an optimum 5 mg/l mass fraction of carbon which is 1.46 times higher than the maximum temperature rise obtained for SAS with TH. For VAS with BH, a maximum temperature rise of 13.1 °C is obtained at an optimum 20 mg/l mass fraction of carbon which is 1.2 times higher than the maximum temperature rise obtained for SAS with BH. For BH a maximum value of Ra is obtained to be 1.12×10^8. On comparing the temperature rise for BH and TH, the temperature rise for VAS with BH is 1.53 times than TH, whereas, for SAS, the BH gives a 1.88 times higher temperature rise than TH. The study concludes that buoyancy forces, Brownian motion, and thermophoresis play an important role in improving the thermal performance of VAS. 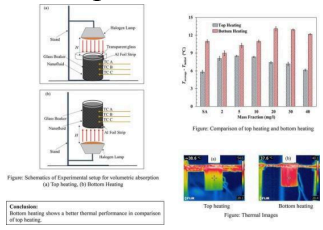
97.	Uranium removal from contaminated groundwater using goethite-loaded composite microporous membrane **M Verma, VA Loganathan** - Science of The Total Environment, 2024 **Abstract:** In this study, we have coupled adsorption and membrane separation for the removal of uranium from contaminated groundwater in environmentally relevant conditions at low energy requirements. The study mainly focuses on elucidating uranium [U(VI)] adsorption mechanisms using surface complexation modeling approach in a novel goethite-loaded composite microfiltration membrane (GLM). The experiments involved immobilizing goethite nanorods in a microporous (0.22 μm pore size) poly (vinylidene fluoride) (PVDF) membrane. The effect of varying goethite loading and hydraulic residence time on U(VI) removal was investigated at field-relevant pH (i.e. pH 8.5). U(VI) adsorption (i.e. 4.95 $\mu g \cdot mg^{-1}$) was optimum at a goethite

	loading of 1.20 mg·cm^{-2}. The effect of varying hydraulic residence time had no impact on U(VI) removal which was also confirmed via performing batch adsorption kinetic experiments. GLM membrane loaded at 1.2 mg·cm^{-2} could treat 275 L of U(VI) contaminated water having 200 µg of U L^{-1} below WHO drinking water limit (i.e. 30 µg of U L^{-1}) with 1 m^2 of membrane surface area at a maximum adsorption capacity of 6.12 µg·mg^{-1}. Varying the pH of aqueous solution, containing U(VI) from pH 4.0 to pH 10.0, showed a significant impact on uranium uptake ranging from 0.7 µg·mg^{-1} to 2.63 µg·mg^{-1} by the composite membrane. The adsorption mechanism of uranium onto goethite was explained via the formation of bidentate surface complexes using the Surface Complexation Model (SCM). The results of batch pH edge experiments and SCM have been compared with pH experiments performed using GLM. The results of SCM predicted the batch pH edge experiment within a RMSE of 0.055. The trend of U(VI) removal in membrane experiments was observed to be similar to that of batch pH edge experiments and was well predicted by the SCM model. Our results show that the novel goethite-loaded membrane has the potential for effective removal of uranium with a lower specific energy consumption. 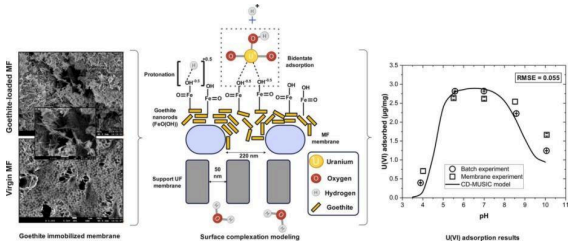
98.	Vulnerable options with regime switching and stochastic liquidity X J He, **P Pasricha**, T Lu, S Lin - The Quarterly Review of Economics and Finance, 2024 **Abstract:** Investigating default risk in pricing options holds significant practical importance, as nearly all market participants and institutions face credit risk. Additionally, economic cycles and asset liquidity are crucial factors that should be incorporated. This paper considers these factors and derives an analytical pricing formula. Specifically, we model the economic cycles through switching volatility driven by a continuous-time Markov chain, while we adopt a discounting factor based on market liquidity levels to model the asset liquidity. We establish a risk-neutral measure after embracing a regime-switching Esscher transform, and formulate a price representation to value vulnerable options analytically despite the complexity of the developed model. We conduct several numerical experiments to validate the model's efficacy and flexibility.
99.	Wiener-lebesgue point property for sobolev functions on metric spaces **MA Bhat, GSR Kosuru** - Mediterranean Journal of Mathematics, 2024 **Abstract:** We establish a Wiener-type integral condition for first-order Sobolev functions defined on a complete, doubling metric measure space supporting a Poincaré inequality. It is stronger than the Lebesgue point property, except for a marginal increase in the capacity of the set of non-Lebesgue points.
100.	Word stress patterns in Dharamshala Tibetan: An optimality theoretic formalization **S Sarkar**, S Kar - Concentric, 2024 **Abstract:** Word stress is a structural property of increasing prominence. An established line of scholarship regarding word stress exists both in terms of theory and description in the Lhasa Tibetan (LT) language. Unlike LT, no such scholarly works are available that focus on Dharamshala Tibetan (DT), a dialectal variety spoken by Tibetan refugees living in the Dharamshala area in Himachal Pradesh, India. The current work aims to provide a systematic and concise theorisation of DT word stress based on the data collected from field in terms of parameters like culminativity, location of the head, direction, and quantity sensitivity. Optimality

	Theory is used to offer a theoretical judgment behind the analysis. A majority of DT words contain a trochaic, weight-insensitive, left-to-right stress pattern. The degenerate foot is accepted. Very few instances of words with an iambic stress pattern were found during the fieldwork. Similarly, few words containing heavy syllables are available in the word stress pattern inventory of DT.

Disclaimer: This publication digest may not contain all the papers published. Library has compiled the publication data as per the alerts received from Scopus and Google Scholar for the affiliation "Indian Institute of Technology Ropar" for the month of November, 2024. The author(s) are requested to share their missing paper(s) details if any, for the inclusion in the next publication digest.